1.7. Flow cytometry

SC-3 cells were plated onto 100 mm-dishes (1.0×10^6 cells/dish) in a protein-free basal medium under an androgen-free condition for synchronization at G1 phase. After incubation for 24 h, the cells were untreated or treated with 10 nM testosterone in the presence or absence of 10 ng/ml TGF-β1 in a serum-free basal medium containing 0.1% bovine serum albumin. At indicated hours, the cells were collected by a cell-scraper, and fixed with 1% paraformaldehyde. The cells were stained with propiodium iodide in a sodium citrate buffer containing 0.1% NP-40 and 10 μg/ml RNase. Then, DNA contents were measured by a BD LSR (BD Biosciences, San Jose, CA, USA).

1.8. Luciferase assay

The nucleotide sequences of the promoter regions for human PSCA (~3.0 kbp) and PSA (~0.55 kbp) were isolated from the database at http://dbtss.hgc.jp, and amplified by genomic PCR. After confirmation of the nuceotide sequencing, the amplified genomic DNAs were subcloned into a pGL-3 luciferase vector (Promega, Madison, WI, USA). The core promoter region of the *fgf8* gene (~0.3 kbp), previously iso-

Table 2
Top 40 of TGF-β-repressive genes in androgen-stimulated SC-3 cells

No.	Genbank accession	Gene symbol	Gene name	Microarray data		
				T[a]	+TGF-β[b]	Ratio
1	D12483	Fgf8	Fibroblast growth factor 8	1620.4	20.5	0.01
2	M32032	Selenbp1	Selenium binding protein 1	535.4	14.8	0.03
3	K02588	Cyp1a1	Cytochrome P450, family 1, subfamily a, polypeptide 1	2384.9	85.9	0.04
4	M17979		Mouse epidermal growth factor binding protein type 1 gene, exons 3–5	264	12.8	0.05
5	J00389	Klk26	Kallikrein 26	212.5	20.2	0.10
6	X15662	Krt2–8	Keratin complex 2, basic, gene 8	627.8	60.7	0.10
7	AF045887	Agt	Angiotensinogen	1201.4	123	0.10
8	AV089850	Aldh3a1	Aldehyde dehydrogenase family 3, subfamily A1	2836.2	323.9	0.11
9	AW049768	Lcn7	Lipocalin 7	6025.2	726.9	0.12
10	D16215	Fmo1	Flavin containing monooxygenase 1	249.4	33.3	0.13
11	AF044030	Ltb4r1	Leukotriene B4 receptor 1	343.1	46.3	0.13
12	AF017128	Fosl1	fos-like antigen 1	5166.2	724.9	0.14
13	AF019385	Hs3st1	Heparan sulfate (glucosamine) 3-O-sulfotransferase 1	648.7	96.1	0.15
14	U07634	Epha2	Eph receptor A2	948.2	147.9	0.16
15	U62674		Mus musculus histone H2a.2–615 (H2a-615), and histone H3.2–615 (H3-615) genes, complete cds	4384.4	725.3	0.17
16	L06047	Gsta4	Glutathione S-transferase, alpha 4	1804.1	309.2	0.17
17	M33988	Pdhb	Pyruvate dehydrogenase (lipoamide) beta	12993	2398	0.18
18	AI326288	Chrne	Cholinergic receptor, nicotinic, epsilon polypeptide	763.9	142.1	0.19
19	M10114	Csnk	Casein kappa	976.9	186.3	0.19
20	M64086	Serpina3n	Serine (or cysteine) proteinase inhibitor, clade A, member 3N	225.7	45	0.20
21	AA590358	2200008D09Rik	RIKEN cDNA 2200008D09 gene	749.3	150.7	0.20
22	D87896	Gpx4	Glutathione peroxidase 4	3747.8	780.8	0.21
23	U44088	Phlda1	Pleckstrin homology-like domain, family A, member 1	2418.4	515.7	0.21
24	U51743	Tead4	TEA domain family member 4	1168.5	252	0.22
25	AW048233	Erf	Ets2 repressor factor	2152.7	476	0.22
26	X78545	Mcpt8	Mast cell protease 8	356.1	78.8	0.22
27	M60523	Idb3	Inhibitor of DNA binding 3	621.5	138.8	0.22
28	AI843448	Mgst3	Microsomal glutathione *S*-transferase 3	3765.3	841	0.22
29	AF090686	Tcn2	Transcobalamin 2	224.7	50.6	0.23
30	AW209486	Psca	Prostate stem cell antigen	505.3	114	0.23
31	Y17709	Fzd9	Frizzled homolog 9 (*Drosophila*)	286.6	65.7	0.23
32	AF064984	Lrp5	Low density lipoprotein receptor-related protein 5	657.2	154.9	0.24
33	U51743	Tead4	TEA domain family member 4	2410.9	575.7	0.24
34	AI845584	Dusp6	Dual specificity phosphatase 6	3317.2	795.5	0.24
35	X61800	Cebpd	CCAAT/enhancer binding protein (C/EBP), delta	7501	1816	0.24
36	L09192	Pcx	Pyruvate carboxylase	1147.3	282	0.25
37	AA241764	Gstm5	Glutathione S-transferase, mu 5	209.9	52	0.25
38	AW047343	Dbp	D site albumin promoter binding protein	335.8	83.3	0.25
39	U88325	Socs1	Suppressor of cytokine signaling 1	1378.8	342.6	0.25
40	U14556	Zfp100	Zinc finger protein 100	318.9	79.4	0.25

[a] T, 10 nM testosterone.
[b] +TGF-β, 10 nM testosterone plus 10 ng/ml of recombinant human TGF-β1.

Table 3
Summary of upregulated genes by TGF-β in androgen-stimulated SC-3 cells

Genbank accession	Gene symbol	Description	Microarray data		
			T[a]	+TGF-β[b]	Ratio
Signal transduction molecule					
AW060401	Arhq	ras homolog gene family, member Q	96.2	1957.8	20.4
AI642553	Iqgap1	IQ motif containing GTPase activating protein 1	47.7	503.8	10.6
X83506	Utrn	Utrophin	29.3	216.2	7.4
D16250	Bmpr1a	Bone morphogenetic protein receptor, type 1A	39.9	294	7.4
U58513	Rock2	Rho-associated coiled-coil forming kinase 2	55.2	354.3	6.4
AW120511	Fbxw7	F-box and WD-40 domain protein 7, archipelago homolog (*Drosophila*)	34.4	216.5	6.3
M89802	Wnt7b	Wingless-related MMTV integration site 7B	243.9	1447.4	5.9
U50413	Pik3r1	Phosphatidylinositol 3-kinase, regulatory subunit, polypeptide 1 (p85 alpha)	47.7	278.9	5.8
U64828	Ncoa1	Nuclear receptor coactivator 1	38	216	5.7
AW060819	Twsg1	Twisted gastrulation homolog 1 (*Drosophila*)	116	627.8	5.4
AI846922	Rasa1	RAS p21 protein activator 1	113.4	594.1	5.2
AF071312	Cops2	COP9 (constitutive photomorphogenic) homolog, subunit 2 (*Arabidopsis thaliana*)	73.9	372.6	5.0
Cytokine, growth factor or growth factor ligand					
D16250	Bmpr1a	Bone morphogenetic protein receptor, type 1A	39.9	294	7.4
M95200	Vegfa	Vascular endothelial growth factor A	158.6	1003.2	6.3
X54542	Il6	Interleukin 6	35.7	203	5.7
Transcriptional factor or modulator					
AA797843	D11Ertd530e	DNA segment, Chr 11, ERATO Doi 530, expressed	11.8	269.1	22.8
AW045443	Mef2a	Myocyte enhancer factor 2A	44.3	702.4	15.9
X53250	Zfa	Zinc finger protein, autosomal	15.9	251.1	15.8
D86603	Bach1	BTB and CNC homology 1	15.8	220.4	13.9
D26532	Runx1	Runt related transcription factor 1	62.9	788	12.5
AF084480	Baz1b	Bromodomain adjacent to zinc finger domain, 1B	20.2	242.8	12.0
AF000294	Pparbp	Peroxisome proliferator activated receptor binding protein	40.7	399.8	9.8
AA867655	Pbl-pending	Polybromo 1/2610016F04Rik: RIKEN cDNA 2610016F04 gene	81.1	529.2	6.5
U09504	Nr1d2	Nuclear receptor subfamily 1, group D, member 2	67.6	429	6.3
AF041822	Tbx15	T-box 15	37	232.7	6.3
AF064088	Tieg1	TGF-β-inducible early growth response 1	148.5	895.7	6.0
X60136	Sp1	*trans*-Acting transcription factor 1	80.4	481.1	6.0
Y07836	Bhlhb2	Basic helix–loop–helix domain containing, class B2	434.9	2503.2	5.8
M64068	Bmi1	B lymphoma Mo-MLV insertion region 1	280	1558.2	5.6
AB024005	Zfp68	Zinc finger protein 68	52.8	285.9	5.4
M63725	Atf1	Activating transcription factor 1	171.6	925.5	5.4
D50416	Six4	Sine oculis-related homeobox 4 homolog (Drosophila)	79.3	415.8	5.2
AF010600	Smarca3	SWI/SNF related, matrix associated, actin-dependent regulator of chromatin, subfamily a, member 3	58.5	304.3	5.2
U21855	Cnot7	CCR4-NOT transcription complex, subunit 7	45	231.5	5.1
D76432	Zfhx1a	Zinc finger homeobox 1a	205.5	1052.2	5.1
Cell cycle control					
AF002823	Bub1	Budding uninhibited by benzimidazoles 1 homolog (*S. cerevisiae*)	12.4	235.9	19.0
AF076845	Hus1	Hus1 homolog (*S. pombe*)	22.7	369.2	16.3
AV138783	Gadd45b	Growth arrest and DNA-damage-inducible 45 beta	62.7	779.3	12.4
Z75332	Stag1	Stromal antigen 1	56.4	391.1	6.9
AI846890	Stag2	Stromal antigen 2	60.4	357.4	5.9
AA032310	Smc4l1	SMC4 structural maintenance of chromosomes 4-like 1 (yeast)	84.2	435.5	5.2
Cell adhesion, extracellular matrix component or modiffer					
AF100777	Wisp1	WNT1-inducible signaling pathway protein 1	72.3	1080.2	14.9
U14135	Itgav	Integrin alpha V	27.2	249.1	9.2
Y13185	Mmp10	Matrix metalloproteinase 10	44.2	364.6	8.2
AF009366	Nedd9	Neural precursor cell expressed, developmentally down-regulated gene 9	143.1	1037	7.2
AF014941	Ctsw	Cathepsin W	84.3	587.7	7.0
U41765	Adam9	A disintegrin and metalloproteinase domain 9 (meltrin gamma)	57	397.3	7.0
AF011379	Adam10	A disintegrin and metalloprotease domain 10	150.9	1041.7	6.9
L18880	Vcl	Vinculin	108.9	633.5	5.8
X66473	Mmp13	Matrix metalloproteinase 13	96.8	558.7	5.8
X62622	Timp2	Tissue inhibitor of metalloproteinase 2	637	3644.5	5.7
M82831	Mmp12	Matrix metalloproteinase 12	59.5	323.5	5.4

[a] T, 10 nM testosterone.
[b] +TGF-β, 10 nM testosterone plus 10 ng/ml of recombinant human TGF-β1.

lated from SC-3 cells [12], was also subcloned into a pGL-3 luciferase vector. The constructed plasmids, pGL-3-hPSCA-luc, pGL-3-hPSA-luc and pGL-3-m*fgf8*-luc, together with the pSV2neo Helper Plasmid (CLONTECH Laboratories, Palo Alto, CA, USA) were transfected into SC-3 cells using a lipofectamine reagent (Invitrogen). The cells were selected in the presence of 400 μg/ml G418 (Invitrogen). After allowing 3 weeks for the selection, the stably expressing SC-3 cells were assayed for the luciferase activity as described previously [12]. The data were standardized per microgram protein as measured by a BCA Protein Assay Kit (Pierce, Rockford, IL, USA).

2. Results

2.1. Oligonucleotide microarray analysis

Compared with the data of the testosterone-stimulated SC-3 cells, 165 genes were up-regulated at more than 5-fold, and 78 genes were down-regulated to less than one-third. The top 40 genes are shown in Tables 1 and 2. High-ranking genes are also categorized by their function or cellular localization in Tables 3 and 4. Functional annotations were provided by Mouse Genome Informatics (http://www.informatics.jax.org/).

Of note, *fgf8* was by far the most responsive gene under the TGF-β1 treatment. Other androgen-regulated genes, such as lipocalin 7 [13], apolipopretein D [14] and PSCA [15], were also repressed by TGF-β1 in this analysis (Table 2 and Supplementary data 2). Along with the TGF-β-mediated growth inhibition of the androgen-stimulated SC-3 cells, $p15^{INK4B}$ was induced by TGF-β1 at up to 3.18-fold, while other *CDKI* genes were constantly or marginally expressed in SC-3 cells (Table 5). In addition, the mouse homologue of Myc-interacting zinc finger protein (Miz)-1, Zfp100, was found to be repressed in this analysis (Table 2), possibly correlating with the $p15^{INK4B}$ induction, as previously reported [16]. As reported in a recent paper [17], the repressions of Id1 and 3 were possibly coupled with TGF-β-mediated

Table 4
Summary of down-regulated genes by TGF-β in androgen-stimulated SC-3 cells

Genbank accession	Gene symbol	Description	Microarray data		
			T[a]	+TGF-β[b]	Ratio
Signal transduction molecule					
U74079	Slc9a3r1	Solute carrier family 9 (sodium/hydrogen exchanger), isoform 3 regulator 1	2648	881.6	0.33
AB004879	Mras	Muscle and microspikes RAS	1026	333.6	0.33
AB021861	Map3k6	Mitogen-activated protein kinase kinase kinase 6	920.1	256	0.28
U20238	Rasa3	RAS p21 protein activator 3	834.2	218.9	0.26
U88325	Socs1	Suppressor of cytokine signaling 1	1379	342.6	0.25
AF064984	Lrp5	Low density lipoprotein receptor-related protein 5	657	154.9	0.24
Y17709	Fzd9	Frizzled homolog 9 (Drosophila)	286.6	65.7	0.23
U07634	Epha2	Eph receptor A2	948.2	147.9	0.16
AF044030	Ltb4r1	Leukotriene B4 receptor 1	343.1	46.3	0.13
Cytokine, growth factor or growth factor ligand					
AJ011967	Gdf15	Growth differentiation factor 15	2523	836.2	0.33
D12483	Fgf8	Fibroblast growth factor 8	1620	20.5	0.01
Transcriptional factor or modulator					
D90085	Zfp144	Zinc finger protein 144	206.4	53.3	0.26
X15784	Myog	Myogenin	264.3	66.6	0.25
U14556	Zfp100	Zinc finger protein 100	319.9	79.4	0.25
AW047343	Dbp	D site albumin promoter binding protein	335.8	83.3	0.25
X61800	Cebpd	CCAAT/enhancer binding protein (C/EBP), delta	7501	1815.6	0.24
AW048233	Erf	Ets2 repressor factor	2153	476	0.22
U51743	Tead4	TEA domain family member 4	1169	252	0.22
AF017128	Fosl1	fos-like antigen 1	5166	724.9	0.14
Cell cycle control					
M31885	Idb1	Inhibitor of DNA binding 1	1301	342.1	0.26
M60523	Idb3	Inhibitor of DNA binding 3	621.5	138.8	0.22
Cell adhesion, extracellular matrix component or modiffer					
AF050666	Gpld1	Glycosylphosphatidylinositol specific phospholipase D1	338.6	103.6	0.31
AW209486	Psca	Prostate stem cell antigen	505.3	114	0.23
X78545	Mcpt8	Mast cell protease 8	356.1	78.8	0.22
AF045887	Agt	Angiotensinogen	1201	123	0.10

[a] T, 10 nM testosterone.
[b] +TGF-β, 10 nM testosterone plus 10 ng/ml of recombinant human TGF-β1.

Table 5
Expression profiles of *CDKI* genes in SC-3 cells

Gene name	Microarray data		
	T[a]	+TGF-β[b]	Ratio
Cyclin-dependent kinase inhibitor 2B (p15)	199.3	633.3	3.18
Cyclin-dependent kinase inhibitor 1B (p27)	43	85.1	1.98
Cyclin-dependent kinase inhibitor 2A (p16)	99.8	153.1	1.53
Cyclin-dependent kinase inhibitor 1C (p57)	20.5	25.2	1.23
Cyclin-dependent kinase inhibitor 2C (p18)	597.8	619.6	1.04
Cyclin-dependent kinase inhibitor 1A (p21)	1504.2	1211.2	0.81
Cyclin-dependent kinase inhibitor 2D (p19)	591.4	301	0.51

[a] T, 10 nM testosterone.
[b] +TGF-β, 10 nM testosterone plus 10 ng/ml of recombinant human TGF-β1.

growth arrest. Other growth-suppressive and apoptotic genes, including growth arrest and DNA-damage-inducible 45 β (GADD45β), TGF-β-inducible early growth response 1 (Tieg1), Fas and caspase 3, were also found in the TGF-β-inducible genes (Table 1 and Supplementary data 1). A well-known TGF-β-responsive gene of plasminogen activator inhibitor (PAI)-1 was also induced at 4.67-fold (data not shown), confirming the TGF-β signaling in SC-3 cells.

A considerable number of cell-matrix remodeling genes, including matrix metalloproteinase (MMP) 10, 12 and 13, disintegrin and metalloproteinase domain (Adam) 9 and 10, and a tissue inhibitor of metalloproteinase (TIMP) 2, were also induced by TGF-β1 in this analysis (Tables 1 and 3 and Supplementary data 1). TGF-β also induced several muscle proteins, such as sarcolemma associated protein (Slmap), utrophin and tropomyosin 4, suggesting the differentiation into mesenchymal or myoepithelial phenotypes in SC-3 cells (Tables 1 and 3 and Supplementary data 1). Other TGF-β-responsive molecules reported in previous microarray data [4,17,18], including Runt-related transcription factor (Runx) 1, vascular endothelial growth factor (VEGF) and IQ motif containing GTPase activating protein (IQGAP) 1, were also found in the TGF-β-inducible genes (Tables 1 and 3 and Supplementary data 1). The up-regulation of WNT1-inducible signaling pathway protein (Wisp)-1 and *Wnt* 7B suggests the activation of Wnt-signaling in response to TGF-β (Tables 1 and 3).

The transcriptional level of the androgen receptor gene was unchanged under the TGF-β treatment in SC-3 cells (data not shown).

2.2. Real-time PCR

Given that FGF8 is a critical factor in the androgen-stimulated growth of SC-3 cells, we further examined the

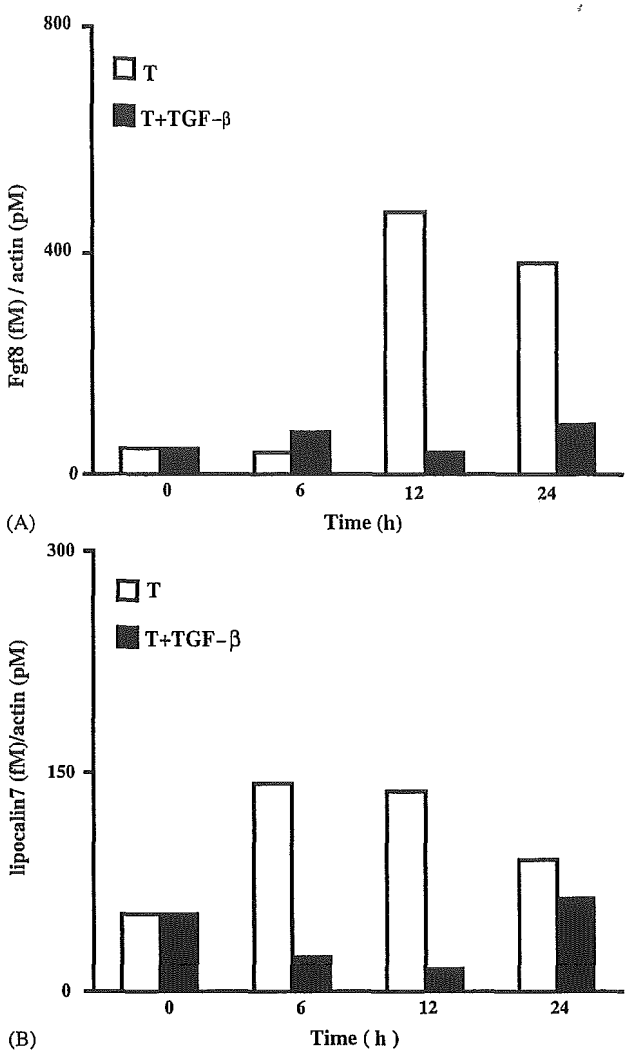

Fig. 1. Real-time PCR analysis on *fgf8* and lipocalin 7 transcripts in testosterone-stimulated SC-3 cells in the absence or presence of TGF-β. SC-3 cells were plated in an androgen-free basal medium, and then stimulated with 10 nM testosterone in the absence (T) or presence of 10 ng/ml TGF-β1 (+TGF-β) under the serum-free condition. RNAs were prepared from SC-3 cells at indicated hours, and the transcriptional levels of *fgf8* (A) and lipocalin 7 (B) were quantitatively analyzed by real-time PCR as described in Section 1.5. The absolute values of the transcripts (fM) were standardized with those of the β-actin transcripts (pM). The results are expressed as the mean of duplicate determinates.

levels of *fgf8* transcripts in the absence or presence of TGF-β1 by real-time PCR. The transcriptional level of *fgf8* in the testosterone-stimulated SC-3 cells reached a 10-fold-induction at 12 h, while its level was severely suppressed in the presence of TGF-β1 (Fig. 1A). Similarly, the transcriptional level of another androgen-regulated gene of lipocalin 7 was also attenuated by TGF-β (Fig. 1B).

2.3. Apoptosis and cell growth analyses

The up-regulation of several apoptotic genes prompted us to investigate the involvement of the apoptotic process in the TGF-β-mediated growth inhibition of SC-3 cells.

The caspase 3 activity remained at marginal levels in the presence of TGF-β1 at 6 and 24 h in SC-3 cells, while TNF-α significantly activated caspase 3 at 6 h (Fig. 2A). In the TUNEL assay, the number of labeled cells was also marginal under the TGF-β1 stimulation at 6 and 24 h, contrasted with the data of the TNF-α treatment in SC-3 cells (Fig. 2B and C). In addition, the treatment with TGF-β1 on androgen-stimulated SC-3 cells showed relative G1-arrest in contrast with the androgen-stimulated control in a flow cytometer (Fig. 2D). All these findings clearly indicate the cell-static effect of TGF-β on the androgen-stimulated SC-3 cells.

Next, we investigated the effect of TGF-β on FGF8-simulated growth in SC-3 cells. The MTT assay clearly demonstrated that TGF-β fails to suppress the FGF8-stimulated growth of SC-3 cells (Fig. 2E). Additional experiment using stably FGF8-expressing SC-3 cells also gave us similar results (Fig. 2F). Both findings strongly

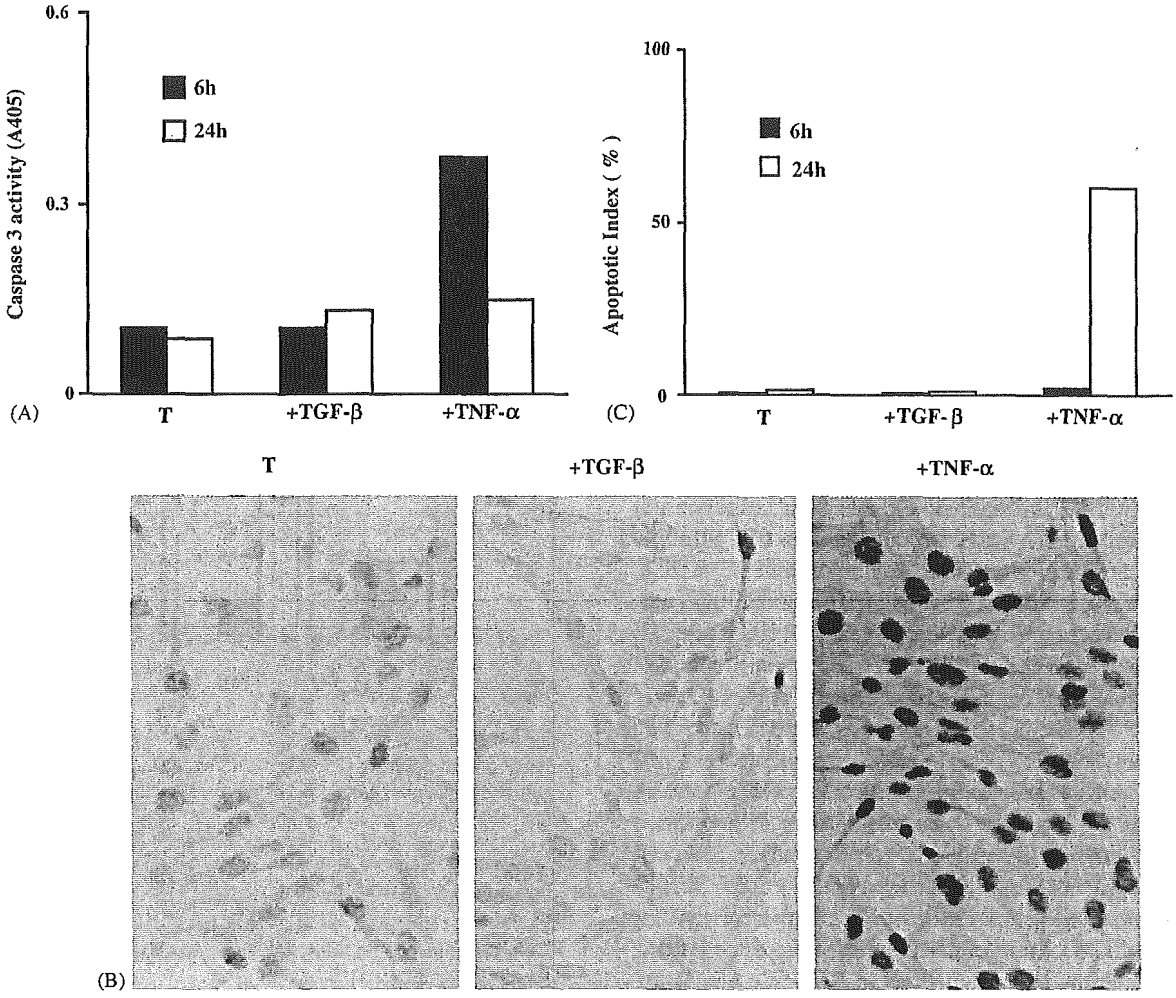

Fig. 2. Apoptosis and cell growth analyses under the TGF-β treatment in SC-3 cells. Effects of TGF-β on the caspase 3 activity in androgen-stimulated SC-3 cells (A). SC-3 cells were plated, and stimulated with 10 nM testosterone in the absence (T) or presence of 10 ng/ml TGF-β1 (+TGF-β). After the indicated hours, the cell lysates were collected, and assayed for caspase 3 activity using the Ac-DEVD-pNA substrate. Analysis of apoptotic processes in response to TGF-β by the TUNEL method (B and C). SC-3 cells were plated, and stimulated with 10 nM testosterone in 4-well-chamber slides in the absence (T) or presence of 10 ng/ml TGF-β1 (+TGF-β). The slides were fixed with 1% paraformaldehyde after the indicated hours of incubation. Cells incorporating digoxigenin-conjugated dNTP at the nucleotide nick ends were detected by peroxidase-based immunocytochemistry. The slides were photographed, and the ratios of positive cells in four different areas were counted. Immunostainings at 24 h are shown in (B). The ratios are expressed as the mean ± S.E.M. (C). In both studies, 5 ng/ml of TNF-α (+TNF-α) was used as the positive control. Flow cytometric analysis (D). SC-3 cells were plated in a protein-free basal medium in the absence of androgen. After incubation for 24 h, the cells were treated or untreated (—) with 10 nM testosterone (T) in the presence or absence of 10 ng/ml TGF-β1 (+ TGF-β). After incubation for 24 h, the cells were collected and fixed with 1% paraformaldehyde. The cells at 0 h were also collected (0 h). After being stained with propiodium iodide, DNA contents were analyzed by a flow cytemeter. Percents of G1 phase were 79.16%; at 0 h, 78.90%; in untreated cells, 33.32%; in testosterone-stimulated cells, 51.55%; in cells treated testosterone plus TGF-β, respectively. Effects of TGF-β on the FGF8-simulated growth of SC-3 cells (E and F). SC-3 cells were plated in an androgen-free basal medium, and then stimulated with 50 ng/ml FGF8 in the presence or absence of various concentrations of TGF-β1 under a serum-free condition (E). Similarly, stably FGF8-expressing SC-3 cells were plated and cultured in the absence or presence of various concentrations of TGF-β1 (F). Cell growth was measured by the MTT method after 72 h of incubation. The results are expressed as the mean ± S.E.M. of triplicate determinants. The other trial showed similar results.

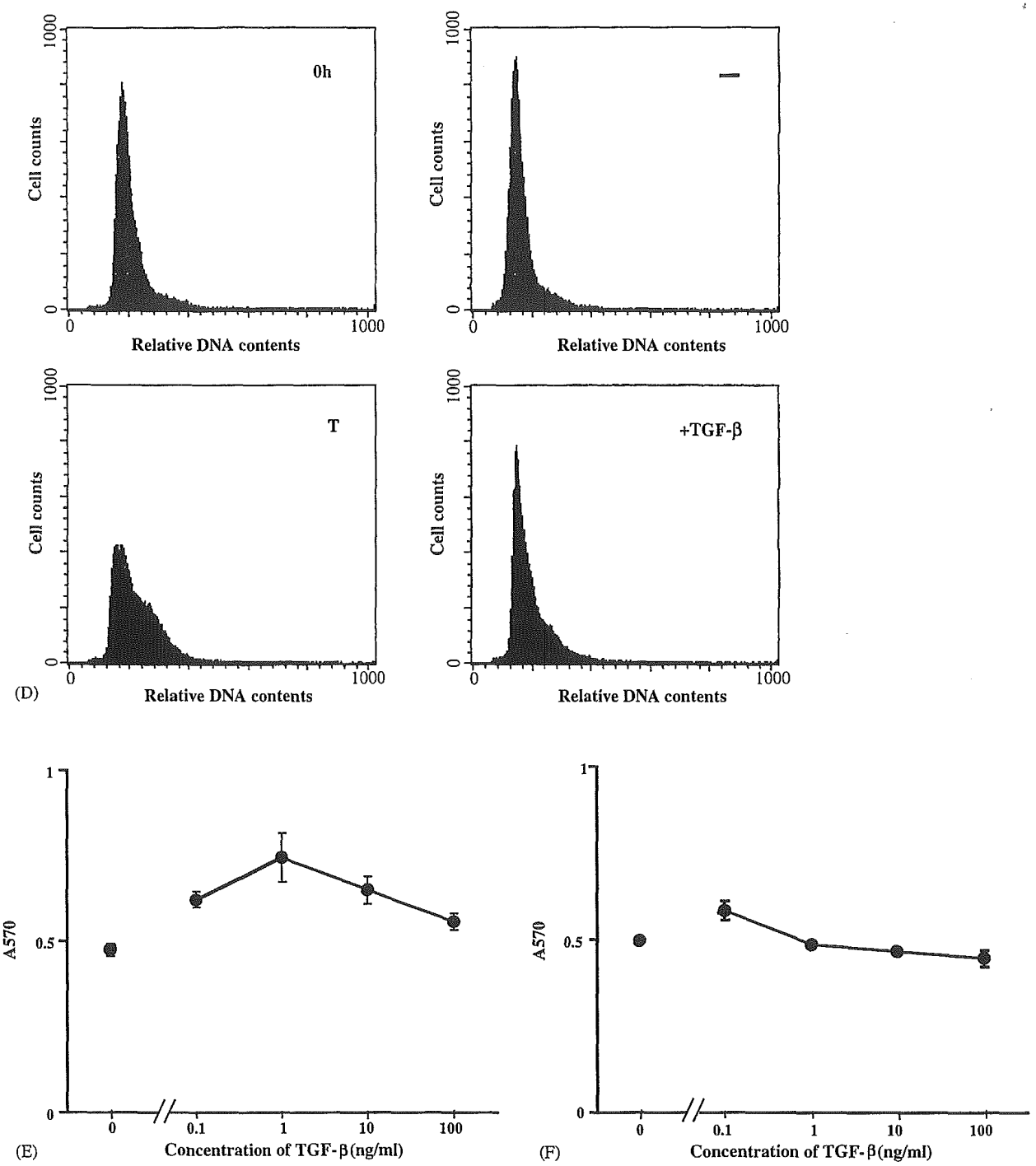

Fig. 2. (*Continued*).

suggest that the transcriptional repression of *fgf8* is required for the TGF-β-mediated growth arrest in SC-3 cells.

2.4. Attenuation of the androgen-responsive promoter activity by TGF-β in SC-3 cells

Next, we investigated the effect of TGF-β on a couple of androgen-responsive promoters. Because the androgen-regulated region in the *fgf8* locus still remains undefined, we used the well-known androgen-responsive promoters of PSA and PSCA in this study. In stably transfected SC-3 cells either with pGL-3-hPSA-luc or pGL-3-hPSCA-luc, the treatment with TGF-β1 significantly suppressed the androgen-responsive reporter activity (Fig. 3A and B). On the other hand, the androgen-unresponsive core promoter activity of the *fgf8* gene was unchanged in the presence of TGF-β (Fig. 3C).

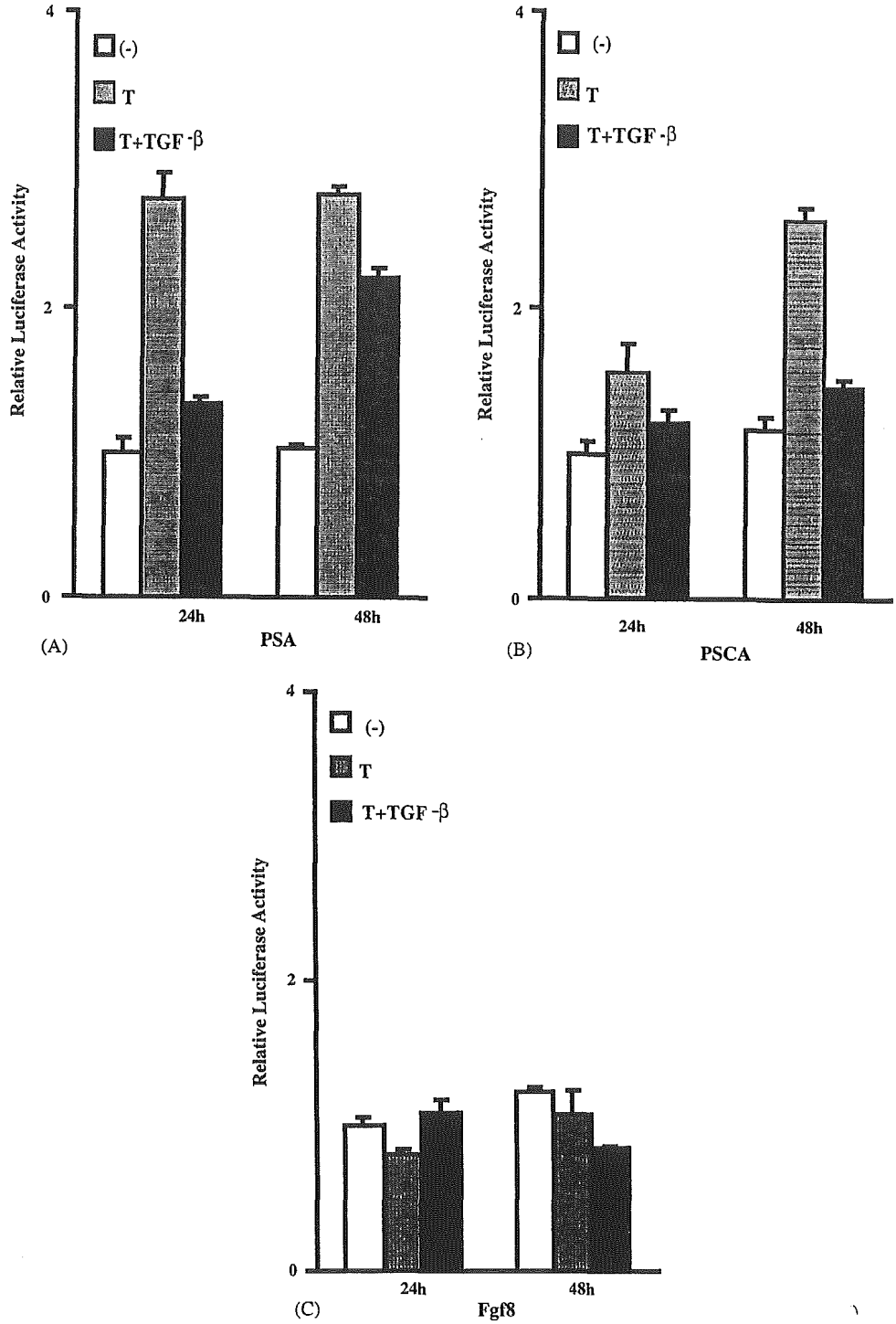

Fig. 3. Effects of TGF-β on the androgen-regulated reporters or the androgen-unresponsive core promoter of the *fgf8* gene in SC-3 cells. SC-3 cells stably transfected with pGL-3-hPSA-luc (A), pGL-3-hPSCA-luc (B), or pGL-3-m*fgf8*-luc (C) were plated and cultured in an unstimulated condition (—), or stimulated with 10 nM testosterone in the absence (T) or presence of TGF-β1 (+TGF-β). After 24 and 48 h of incubation, the cell extracts were collected and assayed for the luciferase activity. Values of luciferase activity were shown as fold ratios with each unstimulated sample at 24 h after standardization with protein concentrations. The results are expressed as the mean ± S.E.M. of triplicate determinants.

3. Discussion

The present microarray analysis clearly demonstrated that *fgf8* was by far the most markedly regulated gene in response to TGF-β in SC-3 cells. The present real-time PCR confirmed the transcriptional repression of *fgf8* by TGF-β. Importantly, *fgf8* is well known as an essential growth factor in the androgen-dependent growth of SC-3 cells. Therefore,

it is highly likely that the repression of *fgf8* is tightly coupled with the TGF-β-mediated growth inhibition in SC-3 cells. Earlier reports have shown that CDKIs and the caspase family are involved in TGF-β-mediated growth inhibition [19,20]. In fact, one of the CDKIs, $p15^{INK4B}$, was induced by TGF-β in SC-3 cells. In addition, apoptotic effector genes of Fas and caspase 3 were also up-regulated by TGF-β in SC-3 cells. Nevertheless, the up-regulation of these molecules was insufficient to lead SC-3 cells to apoptosis within 24 h, as judged by both the TUNEL method and the caspase 3 activity assay. In addition, treatment with TGF-β failed to suppress the cell growth stimulated by exogenous FGF8 in SC-3 cells, suggesting that the transcriptional repression of *fgf8* is required for the TGF-β-mediated growth inhibition. It is very important to elucidate the mechanisms involved in the transcriptional repression of *fgf8* by TGF-β because both growth factors play critical roles on embryogenesis and tumorigenesis. However, our lack of knowledge about the regulatory mechanism of the *fgf8* gene expression by androgens prevents us from taking a direct approach on this issue. Given that the core promoter activity of the *fgf8* gene was not affected by TGF-β in SC-3 cells, it is less possible that a general transcriptional repressor is involved in the repression of *fgf8*. It is rather possible that TGF-β might interrupt the transcriptional cascades induced by androgens, leading to the transcriptional repression of *fgf8*. In support of this notion, the androgen-responsive reporter activity is actually attenuated by TGF-β in SC-3 cells. In fact, a couple of androgen-responsive genes are down-regulated by TGF-β. Based on these findings, it is most likely that some of the androgen-inducible genes are physiological targets of the TGF-β-mediated signaling, and this led us to speculate that the repression of *fgf8* might be directly or indirectly involved in this process.

In recent studies, TGF-β has also been shown to facilitate aggressive and invasive phenotypes in carcinomas through the EMT process [21,22]. The induction of a considerable number of cell-matrix remodeling genes and mesenchymal genes by TGF-β suggests that TGF-β also promotes an EMT phenotype in SC-3 cells. In this sense, SC-3 cells that have escaped from TGF-β-mediated growth arrest might show more aggressive phenotypes through EMT. The cellular balance between the growth-inhibitory effect and the more aggressive phenotype of EMT induced by TGF-β is a next important issue to be explored.

Acknowledgments

We would like to thank Dr. K. Shitara at the Tokyo Research Laboratories of Kyowa Hakko Kogyo for his kind gift of FGF8-expressing plasmid. We also would like to thank Dr. Y. Furukawa at Jichi Medical School and Dr. J. Ohuchi at the Pharmaceutical Research Institute of Kyowa Hakko Kogyo for their helpful advice.

Appendix A. Supplementary data

Supplementary data associated with this article can be found, in the online version, at doi:10.1016/j.jsbmb.2005.01.031.

References

[1] R. Derynck, Y.E. Zhang, Smad-dependent and Smad-independent pathways in TGF-β family signalling, Nature 425 (6958) (2003) 577–584.
[2] M.G. Alexandrow, H.L. Moses, Transforming growth factor β and cell cycle regulation, Cancer Res. 55 (7) (1995) 1452–1457.
[3] J. Massagué, S.W. Blain, R.S. Lo, TGFβ signaling in growth control, cancer, and heritable disorders, Cell 103 (2) (2000) 295–309.
[4] J. Zavadil, M. Bitzer, D. Liang, Y.C. Yang, A. Massimi, S. Kneitz, E. Piek, E.P. Böttinger, Genetic programs of epithelial cell plasticity directed by transforming growth factor-β, Proc. Natl. Acad. Sci. U.S.A. 98 (12) (2001) 6686–6691.
[5] F. Verrecchia, M.L. Chu, A. Mauviel, Identification of novel TGF-β/Smad gene targets in dermal fibroblasts using a combined cDNA microarray/promoter transactivation approach, J. Biol. Chem. 276 (20) (2001) 17058–17062.
[6] S.A. Hayes, M. Zarnegar, M. Sharma, F. Yang, D.M. Peehl, P. ten Dijke, Z. Sun, SMAD3 represses androgen receptor-mediated transcription, Cancer Res. 61 (5) (2001) 2112–2118.
[7] A. Tanaka, K. Miyamoto, N. Minamino, M. Takeda, B. Sato, H. Matsuo, K. Matsumoto, Cloning and characterization of an androgen-induced growth factor essential for the androgen-dependent growth of mouse mammary carcinoma cells, Proc. Natl. Acad. Sci. U.S.A. 89 (19) (1992) 8928–8932.
[8] A. Tanaka, K. Miyamoto, H. Matsuo, K. Matsumoto, H. Yoshida, Human androgen-induced growth factor in prostate and breast cancer cells: its molecular cloning and growth properties, FEBS Lett. 363 (3) (1995) 226–230.
[9] A. Tanaka, A. Furuya, M. Yamasaki, N. Hanai, K. Kuriki, T. Kamiakito, Y. Kobayashi, H. Yoshida, M. Koike, M. Fukayama, High frequency of fibroblast growth factor (FGF) 8 expression in clinical prostate cancers and breast tissues, immunohistochemically demonstrated by a newly established neutralizing monoclonal antibody against FGF 8, Cancer Res. 58 (10) (1998) 2053–2056.
[10] A. Tanaka, T. Kamiakito, N. Takayashiki, S. Sakurai, K. Saito, Fibroblast growth factor 8 expression in breast carcinoma: associations with androgen receptor and prostate-specific antigen expressions, Virchow Arch. 441 (4) (2002) 380–384.
[11] H. Yamanishi, N. Nonomura, A. Tanaka, T. Yasui, Y. Nishizawa, K. Matsumoto, B. Sato, Roles of transforming growth factor β in inhibition of androgen-induced growth of Shionogi carcinoma cells in serum-free medium, Cancer Res. 50 (19) (1990) 6179–6183.
[12] K. Kuriki, T. Kamiakito, H. Yoshida, K. Saito, M. Fukayama, A. Tanaka, Integration of proviral sequences, but not at the common integration sites of the FGF8 locus, in an androgen-dependent mouse mammary Shionogi carcinoma, Cell. Mol. Biol. 46 (7) (2000) 1147–1156.
[13] M. Kobayashi, T. Kinouchi, Y. Hakamata, T. Kamiakito, K. Kuriki, K. Suzuki, A. Tokue, M. Fukayama, A. Tanaka, Isolation of an androgen-inducible novel lipocalin gene, Arg1, from androgen-dependent mouse mammary Shionogi carcinoma cells, J. Steroid Biochem. Mol. Biol. 77 (2–3) (2001) 109–115.
[14] J. Simard, Y. de Launoit, D.E. Haagensen, F. Labrie, Additive stimulatory action of glucocorticoids and androgens on basal and estrogen-repressed apolipoprotein-D messenger, ribonucleic acid levels and secretion in human breast cancer cells, Endocrinology 130 (3) (1992) 1115–1121.

[15] A. Jain, A. Lam, I. Vivanco, M.F. Carey, R.E. Reiter, Identification of an androgen-dependent enhancer within the prostate stem cell antigen gene, Mol. Endocrinol. 16 (10) (2002) 2323–2337.
[16] K. Peukert, P. Staller, A. Schneider, G. Carmichael, F. Hänel, M. Eilers, An alternative pathway for gene regulation by Myc, EMBO J. 16 (18) (1997) 5672–5686.
[17] Y. Kang, C.R. Chen, J. Massague, A self-enabling TGFβ response coupled to stress signaling: Smad engages stress response factor ATF3 for Id1 repression in epithelial cells, Mol. Cell. 11 (4) (2003) 915–926.
[18] L. Xie, B.K. Law, M.E. Aakre, M. Edgerton, Y. Shyr, N.A. Bhowmick, H.L. Moses, Transforming growth factor beta-regulated gene expression in a mouse mammary gland epithelial cell line, Breast Cancer Res. 5 (6) (2003) 187–198.
[19] G.J. Hannon, D. Beach, p15INK4B is a potential effector of TGF-β-induced cell cycle arrest, Nature 371 (6494) (1994) 257–261.
[20] R.H. Chen, T.Y. Chang, Involvement of caspase family proteases in transforming growth factor-β-induced apoptosis, Cell Growth Differ. 8 (7) (1997) 821–827.
[21] W. Cui, D.J. Fowlis, S. Bryson, E. Duffie, H. Ireland, A. Balmain, R.J. Akhurst, TGFβ1 inhibits the formation of benign skin tumors, but enhances progression to invasive spindle carcinomas in transgenic mice, Cell 86 (4) (1996) 531–542.
[22] M. Oft, K.H. Heider, H. Beug, TGFβ signaling is necessary for carcinoma cell invasiveness and metastasis, Curr. Biol. 8 (23) (1998) 1243–1252.

Pathology International 2005; **55**: 63–69

Original Article

Distinct expression patterns of claudin-1 and claudin-4 in intraductal papillary–mucinous tumors of the pancreas

Munetoshi Tsukahara,[1] Hideo Nagai,[1] Tomoko Kamiakito,[2] Hirotoshi Kawata,[2] Norio Takayashiki,[2] Ken Saito[2] and Akira Tanaka[2]

Departments of [1]Surgery and [2]Pathology, Jichi Medical School, Minamikawachi, Kawachi, Tochigi, Japan

The expression of claudin-4 was investigated in human pancreas, pancreatic ductal adenocarcinomas, and intraductal papillary–mucinous tumors of the pancreas (IPMT), and compared with that of claudin-1. In human adult pancreatic specimens, both claudin-1 and claudin-4 were immunohistochemically found in main and branching pancreatic ducts, terminal ductules and acinic cells, with the exception of endocrine cells. Of 12 cases of pancreatic ductal adenocarcinoma, 11 (92%) had positive immunostaining for claudin-4, and seven (58%) for claudin-1. In 44 lesions of 22 cases of IPMT, including six hyperplastic foci distant from the main lesions, clauidin-1 was positive in three out of six (50%) hyperplastic foci, 14 out of 17 (82%) adenomas, three out of 10 (30%) borderline tumors, two out of six (33%) non-invasive carcinomas, and one out of five (20%) invasive carcinomas, producing a statistically negative correlation with histological tumor grades. In contrast, claudin-4 was negative in the six hyperplastic foci, and positive in four out of the 17 (24%) adenomas, five out of the 10 (50%) borderline tumors, five out of the six (83%) non-invasive carcinomas, and four out of the five (80%) invasive carcinomas, producing a statistically positive correlation with histological tumor grades. On study of IPMT subtypes, claudin-1 was positive in nine out of 10 (90%) clear-cell types, seven out of 20 (35%) dark-cell types, and four out of eight (50%) compact-cell types. In contrast, claudin-4 was positive in two out of the 10 (20%) clear-cell types, 13 out of the 20 (65%) dark-cell types, and three out of the eight (38%) compact-cell types. These distinct expression patterns of claudin-1 and claudin-4 suggest that both claudins serve as useful molecular markers for the tumor classification of IPMT.

Correspondence: Akira Tanaka, MD, PhD, Department of Pathology, Jichi Medical School, 3311-1 Yakushiji, Minamikawachi, Kawachi, Tochigi 329-0498, Japan. Email: atanaka@jichi.ac.jp

Received 16 June 2004. Accepted for publication 31 October 2004.

Key words: claudin-1, claudin-4, intraductal papillary-mucinous tumor of the pancreas, pancreas

A tight junction is an intercellular adhesion structure forming a permeability barrier at apical portions, as well as giving cellular polarity to epithelial cells.[1,2] Claudins are essential components of the tight junction, consisting of at least 20 proteins.[3] Given that cellular polarity is frequently distorted in cancers, it is speculated that claudins are dysregulated in various cancers. The overexpression of claudin-3 or claudin-4 has been shown in pancreatic, ovarian, and prostatic cancers.[4–6] In particular, claudin-4 has been reported as playing an important role in the growth, invasion, and metastasis of pancreatic cancers.[7] Pancreatic ductal adenocarcinomas are the most common tumor types in the pancreas, but are also well known for having a very poor prognosis. In contrast, intraductal papillary–mucinous tumors (IPMT) are a distinct entity of pancreatic exocrine tumors.[8] In general, IPMT are subclassified into adenomas, borderline tumors, and carcinomas on the basis of their cellular and structural atypia, and are thought to be subject to an adenoma–carcinoma sequence.[9] In addition, non-invasive IPMT carcinomas have favorable prognoses, compared with pancreatic ductal adenocarcinomas.[9] These characteristics of IPMT prompted us to investigate the correlation between claudin-4 expression and the tumor grades of IPMT. In the present study we used claudin-1 as a comparison. Claudin-1 is the first member of claudins involved in the epidermal barrier formation with claudin-4.[10,11] A recent report has demonstrated the frequent upregulation of claudin-1 in colorectal cancers, suggesting its involvement in gastrointestinal tumorigenesis.[12] In the present study we analyzed claudin-1 and claudin-4 expression in human pancreatic tissues, pancreatic ductal adenocarcinomas, and IPMT using immunohistochemistry and real-time polymerase chain reaction (PCR).

MATERIALS AND METHODS

Samples

Formalin-fixed and paraffin-embedded sections of human pancreas, pancreatic ductal adenocarcinomas, and IPMT were retrieved from the files at Jichi Medical School. The patient profiles of the 22 cases of IPMT are summarized in Table 1. The histological tumor grades were re-evaluated by the three authors (MT, KS and AT). In general, neoplastic lesions without atypia were classified as adenomas, and intraepithelial neoplastic lesions with marked atypia, mostly adjacent to invasive carcinomas, were classified as carcinoma *in situ*. Atypical lesions between the adenoma and carcinoma *in situ* were grouped as borderline tumors. Every histological grade in the 22 cases (38 lesions in total) was investigated. In addition, six hyperplastic foci distant from the main lesions were also investigated. IPMT are also subgrouped into a dark-cell type (nine cases), a clear-cell type (nine cases), and a compact-cell type (four cases) using MUC2 and MUC5AC immunostainings as previously reported.[13] Twelve patients with pancreatic ductal adenocarcinomas (eight with moderately differentiated and four with well-differentiated types) had ages ranging from 53 to 77 years (median, 69.5 years) and a gender ratio of 5:7 (female : male). Three patients with mild pancreatitis, one case from an islet cell tumor, and four cases from carcinomas of the Vater's ampulla or common bile duct were used as normal controls, with ages ranging from 34 to 78 years (median: 55 years), and a gender ratio of 6:2 (female : male). In addition, cDNA specimens (two of ductal carcinomas, four of IPMT, and three of normal pancreatic tissues distant from the main lesion of pancreatic tumors), previously prepared at Jichi Medical School, were used for real-time PCR under the approval of the local ethics committee at Jichi Medical School.

Immunohistochemistry

The monoclonal antibody against human claudin-4, and the polyclonal antibody against human claudin-1 were purchased from Zymed Laboratories (South San Francisco, CA, USA). Formalin-fixed, paraffin-embedded sections were boiled in a microwave oven for 15 min. They were then allowed to interact with each antibody (1:100 dilution for the anticlaudin-1 antibody and 1:400 for the anticlaudin-4 antibody) at 4°C overnight, and stained by an avidin–biotin complex method. The immunostaining results were scored as follows according to a previous report conducted by us:[14] –, negative staining; ±, diffuse weak cytoplasmic staining or focal positive membrane staining; +, distinctly positive membrane staining in more than 20–30% of the tumor areas; ++, strongly positive membrane staining in more than 20–30% of the tumor areas. The categories of '+' and '++' were judged as positive.

Cells

Human pancreatic cancer PANC-1 cells were purchased from Dainippon Pharmacy (Osaka, Japan). PANC-1 cells were maintained in a DMEM medium supplemented with 10% fetal bovine serum (FBS).

Table 1 Patient profiles of IPMT of the pancreas

No.	Age (years)	Gender	Location	Tumor grades	Subtypes
1	65	M	Head	Ad (Hy)	Clear
2	70	M	Body	Ad (Hy)	Clear
3	73	F	Body	Ad (Hy)	Clear
4	56	F	Head	Ad	Clear
5	66	M	Head	Ad	Clear
6	73	M	Body	Ad	Clear
7	72	F	Body	Ad	Clear
8	40	M	Head	Ad	Dark
9	55	M	Body	Ad	Clear
10	56	M	Head	Ad	Compact
11	71	F	Head	Ad, B (Hy)	Compact
12	58	M	Body	Ad, B	Clear
13	75	F	Body	Ad, B	Dark
14	66	F	Head	B, Ad (Hy)	Compact
15	75	M	Body	B, Ad	Dark
16	64	M	Head	B	Dark
17	66	M	Head	B, Ca	Dark
18	70	F	Body	B, Ca, Inv. Ca	Compact
19	53	M	Head	B, Ca, Inv. Ca	Dark
20	74	M	Head	Ca, Inv. Ca, Ad	Dark
21	62	F	Body	Ca, Inv. Ca, B, Ad (Hy)	Dark
22	70	M	Head	Ca, Inv. Ca	Dark

Tumor grades: Ad, adenoma; B, borderline lesions; Ca, non-invasive carcinoma; Inv. Ca, invasive carcinoma. The main lesion is represented at the top. Six hyperplastic foci distant from tumors (Hy) were also investigated. IPMT, intraductal papillary–mucinous tumor: clear, clear-cell type; dark, dark-cell type; compact, compact-cell type.

RNA

PANC-1 cells (70×10^4/well) were plated in a DMEM medium supplemented with 2% FBS treated with dextran-coated charcoal (DCC). The next day, the cells were cultured in the absence or presence of 10 ng/mL recombinant human transforming growth factor (TGF)-β1 (R&D Systems, Mineapolis, MN, USA) in the DMEM medium supplemented with 2% DCC-treated FBS. After a 48 h incubation, total cellular RNA were prepared from the cells using a TRIzol reagent (Invitrogen, Carlsbad, CA, USA).

Real-time polymerase chain reaction

The nine aforementioned cDNA samples were cycled for PCR by an ABI PRISM 7700 (Applied Biosystems, Foster City, CA, USA), monitoring the signals from TaqMan probes. Primer sets used were: human claudin-1 forward primer, 5′-TACTCCTATGCCGGCGACA-3′; reverse primer, 5′-GACATCCACAGCCCCTCGT-3′; TaqMan primer, Fam-CGTGACCGCCCAGGCCATG-Tamra; human claudin-4 forward primer, 5′-CATCGGCAGCAACATTGTCA-3′; reverse primer, 5′-GCACCTTACACGTAGTTGCT-3′; TaqMan primer, Fam-TGGTGCAGAGCACCGGCCA-Tamra; human β-actin forward primer; 5′-TGAGCGCGGCTACAGCTT-3′; reverse primer, 5′-TCCTTAATGTCACGCACG-3′; and TaqMan primer, Fam-ACCACCACGGCCGAGCGG-Tamra.

Statistics

Data were statistically analyzed using Statcel software (OMS, Tokyo, Japan).

RESULTS

Immunohistochemistry findings

In human adult pancreatic tissues, both claudin-1 and claudin-4 had clear membrane immunostainings in acinar cells (Fig. 1a,b). Positive immunostainings for claudin-1 and claudin-4 were also found in branching pancreatic ducts and terminal ductules, but the intensity was weaker than that of acinar cells (Fig. 1a,b and data not shown). The signals for claudin-1 and claudin-4 were absent in islet cells (data not shown). In addition, positive immunostainings for claudin-1 and claudin-4 were also found in the main pancreatic duct of the ampulla region, although the expression patterns were somewhat different from each other. The claudin-1-positive cells were mainly found in the glandular cells, while the claudin-4-positive cells were found mainly in the surface epithelial cells (Fig. 1c,d).

Of 12 cases of ductal adenocarcinomas, 11 (92%) were positive for claudin-4 and seven (58%) for claudin-1 (Fig. 1e,f; Table 2). Although claudin-4 had clear and membranous stainings in most cases, and despite the rather weak stainings of claudin-1, there was no statistical significance between claudin-1 and claudin-4 expressions by Mann–Whitney *U*-test.

Of 17 IPMT adenoma lesions, 14 (82%) were positive for claudin-1, while four (24%) were positive for claudin-4 (Fig. 2a–c; Table 2). In contrast with the adenoma data, out of six non-invasive carcinoma lesions, three (50%) were positive for claudin-1, and five (83%) were positive for claudin-4 (Fig. 2g–i; Table 2). In invasive carcinoma lesions, one out of five (20%) was positive for claudin-1, and four (80%) were positive for claudin-4. There was no stastical difference of the immunostainings between non-invasive and invasive carcinomas. In addition, three out of 10 borderline lesions (30%) were positive for claudin-1, and five (50%) were positive for claudin-4, three out of six hyperplastic foci (50%) were positive for claudin-1, and none was positive for claudin-4 (Fig. 2d–f; Table 2). The immunostaining pattern of claudin-4 had a statistically positive correlation, while that of claudin-1 had a negative correlation between the immunostaining pattern and the histological tumor grades by the Spearman correlation coefficient rank test.

The immunohistochemical data of the 38 IPMT lesions excepting six hyperplastic foci were re-analyzed according to the subtypes. Nine out of 10 lesions (90%) in clear-cell types were positive for claudin-1, while two (20%) were positive for claudin-4 (Fig. 2a–c; Table 3). In contrast, seven out of 20

Table 2 Claudin-1 and claudin-4 in ductal adenocarcinomas and IPMT

	Claudin-1 immunoreactivity						Claudin-4 immunoreactivity					
	Total	–	±	+	++	Positive (%)	Total	–	±	+	++	Positive (%)
Ductal adenocarcinoma	12	2	3	5	2	58	12	1	0	6	5	92
IPMT												
Hyperplasia	6	1	2	1	2	50	6	4	2	0	0	0
Adenoma	17	1	2	5	9	82	17	10	3	4	0	24
Borderline	10	2	5	3	0	30	10	2	3	3	2	50
Carcinoma	6	0	4	2	0	33	6	0	1	1	4	83
Invasive carcinoma	5	2	2	1	0	20	5	0	1	2	2	80

IPMT, intraductal papillary–mucinous tumor.

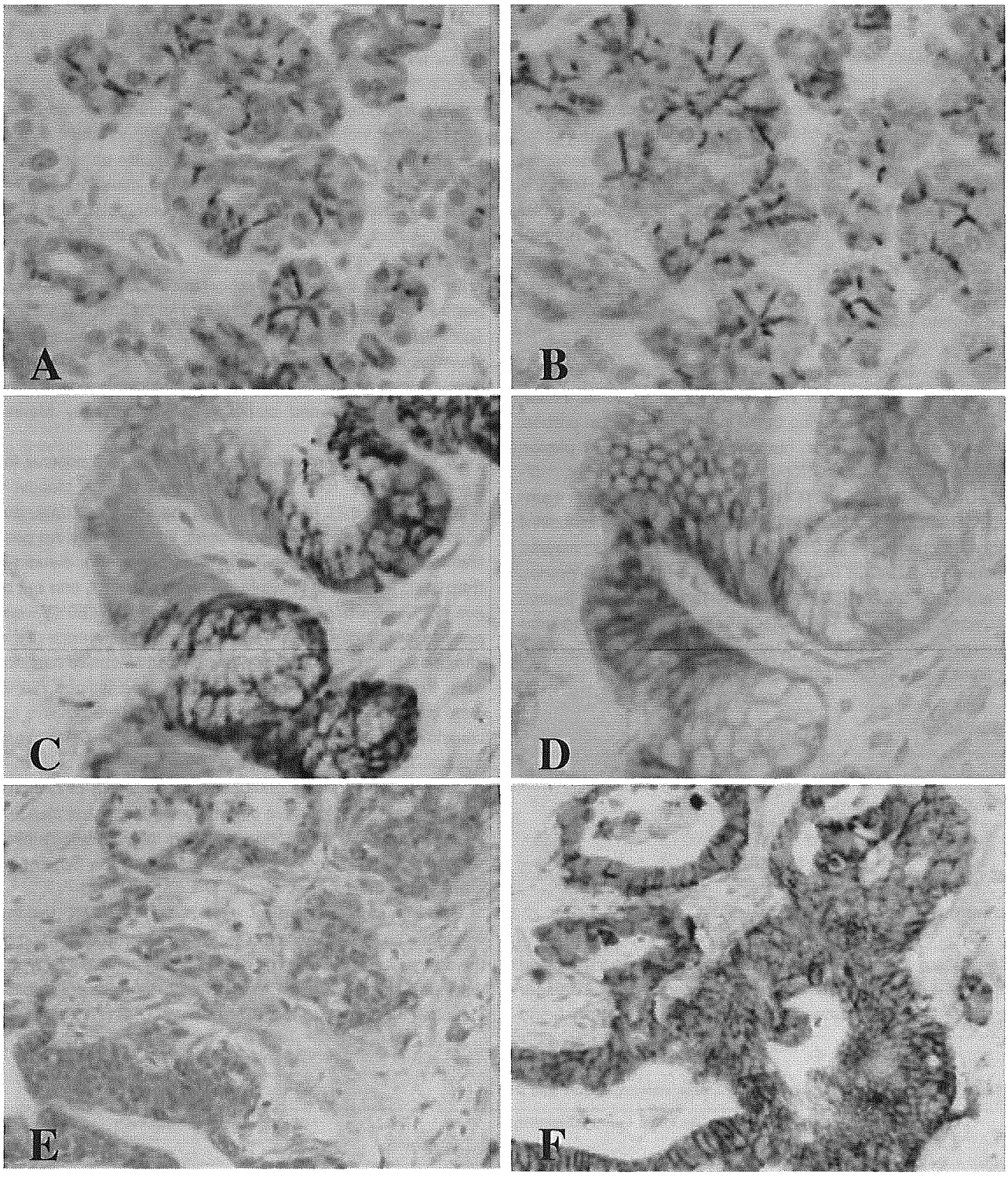

Figure 1 Claudin-1 and claudin-4 immunostainings in human adult pancreatic tissues and pancreatic ductal carcinomas. (**A,B**) Claudin-1 and claudin-4 immunostainings in the peripheral pancreatic tissue. Membranous immunostainings were distinctly found in acinar cells, and weakly in ductal epithelia of human adult pancreatic tissues (**A**, claudin-1; **B**: claudin-4). (**C,D**) Claudin-1 and claudin-4 immunostainings in the main pancreatic duct. In the main pancreatic duct, the immunostaining of claudin-4 was mainly found in the surface epithelia, while that of claudin-1 was in the glandular portions (**C**, claudin-1; **D**, claudin-4). (**E,F**) Claudin-1 and claudin-4 immunostainings in the pancreatic ductal adenocarcinoma. Membranous immunostaining was marked in ductal adenocarcinoma cells for claudin-4, but less for claudin-1 (**E**, claudin-1; **F**, claudin-4).

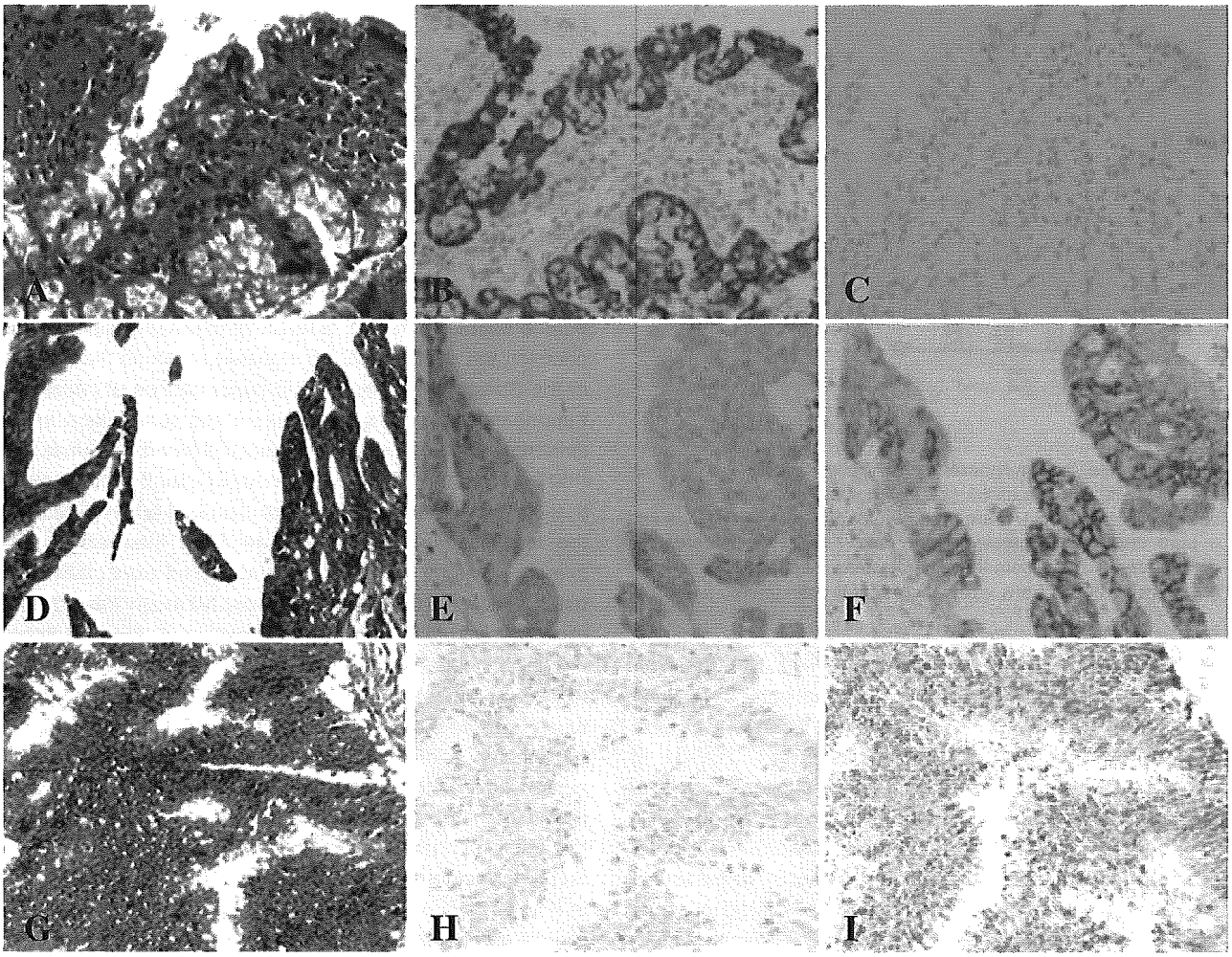

Figure 2 Claudin-1 and claudin-4 immunostainings in intraductal papillary and mucinous tumors (IPMT). (**A–C**) Claudin-1 and claudin-4 immunostainings in the clear-cell type of IPMT adenoma. The immunostaining of claudin-1 was marked, but that of claudin-4 was completely absent (**A**, HE; **B**, claudin-1; **C**, claudin-4). (**D–F**) Claudin-1 and claudin-4 immunostainings in the compact-cell type of borderline tumor. Claudin-1 showed focal and cytoplasmic immunostaining, while claudin-4 showed clear membranous immunostaining mainly in the claudin-1-negative cells (**D**, HE; **E**, claudin-1; **F**, claudin-4). (**G–I**) Immunostainings of claudin-1 and claudin-4 in the dark-cell type of IPMT carcinoma. Immunostaining of claudin-4 was marked in the lateral membranes of most carcinoma cells, but that of claudin-1 was absent in the lateral membranes (**G**, HE; **H**, claudin-1; **I**, claudin-4).

Table 3 *Claudin-1 and claudin-4 in the subtypes of IPMT*

		Claudin-1 immunoreactivity				Claudin-4 immunoreactivity			
	Total	–	±	+	++	–	±	+	++
Clear	10	0	1	2	7	7	1	2	0
Dark	20	3	10	6	1	4	3	5	8
Compact	8	2	2	3	1	1	4	3	0

IPMT, intraductal papillary–mucinous tumor.

lesions (35%) in dark-cell types were positive for claudin-1, while 13 (65%) were positive for claudin-4 (Fig. 2g–i; Table 3). In compact-cell types, four out of eight lesions (50%) were positive for claudin-1, and three (38%) were positive for claudin-4 (Fig. 2d–f; Table 3). The immunohistochemical results of both claudins were statistical different among the IPMT subtypes by Kruskal–Wallis test.

Real-time polymerase chain reaction

We first tested the real-time PCR conditions using human pancreatic cancer PANC-1 cells. The transcriptional level of claudin-4 was prominent in PANC-1 cells, reaching up to 8.4×10^5 fmol/pmol. Concordant with a previous report,[7] the transcriptional level of claudin-4 was drastically decreased, to 0.2% of the unstimulated level, when PANC-1 cells were

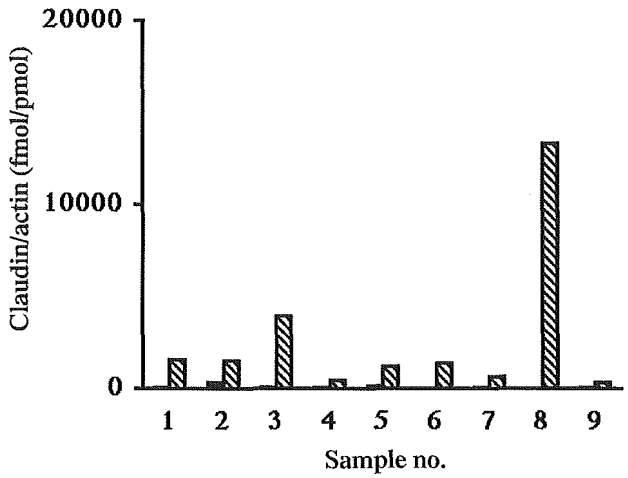

Figure 3 Real-time polymerase chain reaction (PCR) analysis of claudin-1 (■) and claudin-4 (▨) in surgically resected pancreatic specimens. Samples 1–3 are from normal pancreatic tissues, 4 and 5 from ductal adenocarcinomas, 6 and 7 from IPMT borderline tumors, and 8 and 9 from IPMT carcinomas. Absolute values (fmol) are adjusted by the transcriptional level of β-actin (pmol).

treated with 10 ng/mL of recombinant TGF-β1. The transcriptional level of claudin-1 was 1.9×10^4 fmol/pmol in PANC-1 cells, much lower than that of claudin-4. Its level was also decreased to 1.8×10^3 fmol/pmol in response to TGF-β1. In surgically resected specimens, the transcriptional levels of claudin-1 and claudin-4 were much lower than those in PANC-1 cells: on the order of 1.0×10^3 fmol/pmol in claudin-4 and 1.0×10^2 fmol/pmol in claudin-1 (Fig. 3). In particular, the lower levels of ductal carcinoma cases suggest some difficulties in sampling because of the rich stromal components in pancreatic ductal adenocarcinomas. Nevertheless, one specimen of IPMT carcinoma expressed a higher level of claudin-4 (Fig. 3).

DISCUSSION

Here we present the distinct expression patterns of claudin-1 and claudin-4 in pancreatic tissues, ductal adenocarcinomas, and IPMT. Both claudin-1 and claudin-4 showed strong membranous immunostainings in acinar cells and mild immunostainings in ductal cells from adult pancreatic tissues. Interestingly, the expression patterns of claudin-1 and claudin-4 were considerably varied in ductal adenocarcinomas and IPMT. In particular, the expression of claudin-1 or claudin-4 was negatively or positively correlated with the histological tumor grades of IPMT. Recent reports have shown that the expression of claudin-1 and claudin-4 is altered under various conditions. For example, an oncogenic *Raf* signal suppresses the expression of claudin-1 in a rat salivary gland epithelial cell line, while the blockade of the *Ras* signal leads to the downregulation of claudin-4 in human pancreatic cancers PANC-1.[7,15] Importantly, it is well known that the *K-ras* mutaion is found in most cases of pancreatic cancers and in considerable cases of IPMT.[16–18] These reported findings allow us to speculate that the dysregulations of claudin-1 and claudin-4 in the present study might be, at least in part, coupled with the activation of the *Ras–Raf* pathway in pancreatic cancers and IPMT carcinomas. In addition, the claudin-4 expression was severely repressed in response to TGF-β in human pancreatic cancer PANC-1 cells. Therefore, it is likely that the downregulation of claudin-4 in IPMT adenomas might be, in part, a result of the TGF-β signaling. In contrast, the deficient TGF-β signaling, such as the deletion of the *Smad 4* gene, one of the major causes of pancreatic tumorigenesis,[19] might also make some contribution to the overexpression of claudin-4 in ductal adenocarcinomas and IPMT carcinomas. From these points of view it seems natural that the expression of claudin-1 or claudin-4 is correlated with the histological tumor grades of IPMT. Interestingly, the immunostainings of claudin-1 and claudin-4 were statistically different among the IPMT subtypes. Although the previous report has mentioned the overexpression of claudin-1 in colorectal cancers,[12] the claudin-1 expression seemed to be higher in IPMT clear-cell types (gastric types) than dark-cell types (intestinal types) in the present study. In addition, our preliminary analysis showed that claudin-4 is strongly expressed in both intestinal and gastric types of gastric adenocarcinomas. Although further studies would be required, the epithelial phenotypes were likely to make some contribution to the preferential expression of claudin-1 and claudin-4 in IPMT. The lack of any statistical significance between the claudin-1 and claudin-4 immunostainings in ductal adenocarcinomas may result from further gene mutations or cellular signaling alterations during tumorigenesis.

Very recently, claudin-4 has been shown to be one of the molecular markers of the invasive phenotypes of IPMT through gene expression profiling.[20] In contrast, it has been also reported that claudin-4 decreases invasiveness and metastatic potential of pancreatic cancers.[7] In addition, other reports have shown that several claudins are involved in cancer progression through the activation of matrix metalloproteinase (MMP)-2.[21,22] To date, the biological significance of the claudin-4 overexpression in pancreatic carcinomas has not been fully understood. Nevertheless, as a receptor of *Clostridium perfringens* enterotoxin (CPE), claudin-4 has become an attractive molecule for a CPE-mediated cytolytic cancer therapy. A number of reports have pointed out the anticancer effects of CPE through claudin-4.[4,23] Although the present real-time PCR failed to demonstrate any correlation between the levels of claudin-1 or claudin-4 and the histological tumor grades, future diagnostic applications for the real-time PCR method will provide useful information about the CPE-mediated therapy.

ACKNOWLEDGMENTS

We would like to thank Dr Sata at Jichi Medical School for his helpful discussions. We also thank M. Mizogami, M. Yanagita, K. Honmou, S. Sato, K. Hidano, M. Kikuchi, M. Hoshino, and Y. Haga for their technical assistance.

REFERENCES

1 Tsukita S, Furuse M, Itoh M. Multifunctional strands in tight junctions. *Nat Rev Mol Cell Biol* 2001; **2**: 285–93.
2 Tsukita S, Furuse M. Claudin-based barrier in simple and stratified cellular sheets. *Curr Opin Cell Biol* 2002; **14**: 531–6.
3 Katoh M, Katoh M. CLDN23 gene, frequently down-regulated in intestinal-type gastric cancer, is a novel member of CLAUDIN gene family. *Int J Mol Med* 2003; **11**: 683–9.
4 Michl P, Buchholz M, Rolke M *et al.* Claudin-4: a new target for pancreatic cancer treatment using *Clostridium perfringens* enterotoxin. *Gastroenterology* 2001; **121**: 678–84.
5 Rangel LBA, Agarwal R, D'Souza T *et al.* Tight junction proteins claudin-3 and claudin-4 are frequently overexpressed in ovarian cancer but not in ovarian cystadenomas. *Clin Cancer Res* 2003; **9**: 2567–75.
6 Long H, Crean CD, Lee W-H, Cummings OW, Gabig TG. Expression of *Clostridium perfringens* enterotoxin receptors claudin-3 and claudin-4 in prostate cancer epithelium. *Cancer Res* 2001; **61**: 7878–81.
7 Michl P, Barth C, Buchholz M *et al.* Claudin-4 expression decreases invasiveness and metastatic potential of pancreatic cancer. *Cancer Res* 2003; **63**: 6265–71.
8 Sessa F, Solicia E, Capella C *et al.* Intraductal papillary-mucinous tumours represent a distinct group of pancreatic neoplasma: an investigation of tumour cell differentiation and K-ras, p53 and c-erbB-2 abnormalities in 26 patients. *Virchows Arch* 1994; **425**: 357–67.
9 Solcia E, Capella C, Klöppel G, eds. *Tumors of the Pancreas.* Washington, DC: Armed Forces Institute of Pathology, 1995.
10 Furuse M, Fujita K, Hiiragi T, Fujimoto K, Tsukita S. Claudin-1 and -2: novel integral membrane proteins localizing at tight junctions with no sequence similarity to occludin. *J Cell Biol* 1998; **141**: 1539–50.
11 Furuse M, Hata M, Furuse K *et al.* Claudin-based tight junctions are crucial for the mammalian epidermal barrier: a lesson from claudin-1-deficient mice. *J Cell Biol* 2002; **156**: 1099–111.
12 Miwa N, Furuse M, Tsukita S, Niikawa N, Nakamura Y, Furukawa Y. Involvement of claudin-1 in the beta-catenin/Tcf signaling pathway and its frequent upregulation in human colorectal cancers. *Oncol Res* 2000; **12**: 469–76.
13 Yonezawa S, Nakamura A, Horinouchi M, Sato E. The expression of several types of mucin is related to the biological behavior of pancreatic neoplasms. *J Hepatobiliary Pancreat Surg* 2002; **9**: 328–41.
14 Fujii A, Kamiakito T, Takayashiki N, Fujii T, Tanaka A. Neuroendocrine tissue-specific transcription factor, BETA2/NeuroD, in gastric carcinomas: a comparison with chromogranin A and synaptophysin expressions. *Pathol Res Prac* 2003; **199**: 513–19.
15 Li D, Mrsny RJ. Oncogenic Raf-1 disrupts epithelial tight junction via downregulation of occludin. *J Cell Biol* 2000; **148**: 791–800.
16 Smit VT, Boot AJ, Smits AM, Fleuren GJ, Cornelisse CJ, Bos JL. KRAS codon 12 mutations occur very frequently in pancreatic adenocarcinomas. *Nucleic Acids Res* 1988; **16**: 7773–82.
17 Griffin CA, Hruban RH, Morsberger LA *et al.* Consistent chromosome abnormalities in adenocarcinoma of the pancreas. *Cancer Res* 1995; **55**: 2394–9.
18 Yoshizawa K, Nagai H, Sakurai S *et al.* Clonality and K-ras mutation analyses of epithelia in intraductal papillary mucinous tumor and mucinous cystic tumor of the pancreas. *Virchows Arch* 2002; **441**: 437–43.
19 Shutte M, Hruban RH, Hedrick L *et al.* DPC4 gene in various tumour types. *Cancer Res* 1996; **56**: 2527–30.
20 Sato N, Fukushima N, Maitra A *et al.* Gene expression profiling identifies genes associated with invasive intraductal papillary mucinous neoplasms of the pancreas. *Am J Pathol* 2004; **164**: 903–14.
21 Miyamori H, Takino T, Kobayashi Y *et al.* Claudin promotes activation of pro-matrix metalloproteinase-2 mediated by membrane-type matrix metalloproteinases. *J Biol Chem* 2001; **276**: 28 204–11.
22 Ellenrieder V, Alber B, Lacher U *et al.* Role of MT-MMPs and MMP-2 in pancreatic cancer progression. *Int J Cancer* 2000; **85**: 14–20.
23 Kominsky SL, Vali M, Korz D *et al. Clostridium perfringens* enterotoxin elicits rapid and specific cytolysis of breast carcinoma cells mediated through tight junction proteins claudin 3 and 4. *Am J Pathol* 2004; **164**: 1627–33.

A Neutralizing Anti–Fibroblast Growth Factor 8 Monoclonal Antibody Shows Potent Antitumor Activity against Androgen-Dependent Mouse Mammary Tumors *In vivo*

Naoki Shimada,[1] Toshihiko Ishii,[2] Teruyoshi Imada,[2] Katsumi Takaba,[2] Yuka Sasaki,[1] Kumiko Maruyama-Takahashi,[1] Yoshimi Maekawa-Tokuda,[2] Hideaki Kusaka,[2] Shiro Akinaga,[2] Akira Tanaka,[3] and Kenya Shitara[1]

Abstract

Purpose: Fibroblast growth factor 8b (FGF8b) has been implicated in oncogenesis of sex hormone–related malignancies. A murine monoclonal anti-FGF8 antibody, KM1334, has been raised against a FGF8b-derived peptide and shown to neutralize FGF8b activity in an androgen-dependent mouse mammary cell line (SC-3) *in vitro* growth. The purpose of this study was to evaluate KM1334 as a therapeutic agent for FGF8-dependent cancer.

Experimental Design: Specificity and neutralizing activity of KM1334 were examined *in vitro*. *In vivo* therapeutic studies were done in nude mice bearing SC-3 tumors s.c.

Results: KM1334 recognized FGF8b and FGF8f specifically out of four human FGF8 isoforms and showed little binding to other members of FGF family. Neutralizing activity of KM1334 was confirmed by both blocking of FGF8b binding to its three receptors (FGFR2IIIc, FGFR3IIIc, and FGFR4) and FGF8b-induced phosphorylation of FGFR substrate 2α and extracellular signal-regulated kinase 1/2 in SC-3 cells. The *in vitro* inhibitory effect could be extended to *in vivo* tumor models, where KM1334 caused rapid regression of established SC-3 tumors in nude mice. This rapid regression of tumors after KM1334 treatment was explained by two independent mechanisms: (*a*) decreased DNA synthesis, as evidenced by a decrease in uptake of 5-bromo-2′-deoxyuridine, and (*b*) induction of apoptosis as shown by the terminal deoxynucleotidyl transferase–mediated nick end labeling assay.

Conclusions: KM1334 possesses strong blocking activity *in vitro* and antitumor activity *in vivo* and therefore may be an effective therapeutic candidate for the treatment of cancers that are dependent on FGF8b signaling for growth and survival.

Since the discovery of monoclonal antibody (mAb) technology (1), attempts have been made to use their exquisite specificity and affinity for the treatment of human diseases, such as cancer. In recent years, significant advances have been made in the therapeutic use of antibodies as shown by the growing numbers that are gaining approval for clinical use (2). Many targets for therapeutic antibodies are membrane-bound antigens, which is necessary for antibodies to show effector functions, such as antibody-dependent cellular cytotoxicity and complement-dependent cytotoxicity. However, soluble molecules, which promote tumor progression directly or indirectly, can also be good targets for cancer therapy. For example, bevacizumab, an anti-vascular endothelial growth factor neutralizing antibody, showed clinical benefits for patients with metastatic colorectal cancer in phase III study (3). For the clinical application of mAbs against growth factors, candidate mAbs having high specificity, potent neutralizing activity, and *in vivo* antitumor activity should be selected for the further development of humanized antibodies.

The fibroblast growth factors (FGF) form a family of at least 24 growth-regulatory proteins. They share 35% to 50% amino acid sequence identity and induce proliferation and differentiation in a wide range of cells of epithelial, mesodermal, and neuroectodermal origin (4, 5). FGF8 was originally isolated from the conditioned medium of an androgen-dependent mouse mammary tumor cell line (SC-3) as an androgen-induced growth factor and was later classified as a member of the FGF family based on structural similarity (6). FGF8 has been found to have an important role in embryogenesis and morphogenesis (7). It is expressed during gastrulation, in brain development, and in the process of limb and facial morphogenesis of the developing mouse (8–13). FGF8 has been identified as an oncogene product based on its transforming activity in NIH3T3 cells (14). In addition, a high frequency of

Authors' Affiliations: [1]Tokyo Research Laboratories, Kyowa Hakko Kogyo Co., Ltd., Tokyo, Japan; [2]Drug Development Research Laboratories Pharmaceutical Research Institute, Kyowa Hakko Kogyo Co., Ltd., Shizuoka, Japan; and [3]Department of Pathology, Jichi Medical School, Tochigi, Japan

Received 11/18/04; revised 2/16/05; accepted 2/17/05.

The costs of publication of this article were defrayed in part by the payment of page charges. This article must therefore be hereby marked *advertisement* in accordance with 18 U.S.C. Section 1734 solely to indicate this fact.

Requests for reprints: Kenya Shitara, Tokyo Research Laboratories, Kyowa Hakko Kogyo, Co., Ltd., 3-6-6 Asahi-machi, Machida, Tokyo 194-8533, Japan. Phone: 81-42-725-0857; Fax: 81-42-725-2689; E-mail: kshitara@kyowa.co.jp.

FGF8 mRNA overexpression, which is associated with decreased patient survival and persists in androgen-independent disease, was detected by tissue *in situ* hybridization in prostate cancer specimens (15).

The structure of the *FGF8* gene is more complicated than that of the other members of the FGF family. Alternative splicing of the *FGF8* gene potentially gives rise to eight different protein isoforms (a-h) in mice and four isoforms (a, b, e, and f) in humans (6, 16, 17). The isoforms differ in the NH_2 terminus. The biological function of these forms is not exactly known, but at least they differ in transforming potential. FGF8b has been found to have the highest NIH3T3 cell-transforming capacity (18, 19). Furthermore, transgenic mice overexpressing FGF8b in the mammary glands are found to develop mammary tumor and those in prostate epithelial cells develop prostatic intraepithelial neoplasia (20, 21). Overexpression of FGF8b gives a more aggressive phenotype, including increased growth rate to cultured human prostate and breast cancer cells (22, 23). Upregulation of FGF8b was also observed in multiple human cancers, such as prostate, breast, and ovary carcinomas (24–28). The above findings strongly suggest that FGF8, especially FGF8b, is the potential target for antibody-based cancer therapy.

FGF signaling is transduced through the formation of a complex of a growth factor, a proteoglycan, and a high-affinity FGF receptor (FGFR), which is a transmembrane tyrosine kinase receptor (29). Four different high-affinity receptors (FGFR1, FGFR2, FGFR3, and FGFR4) bind FGF ligands and display varying patterns of expression (reviewed in refs. 1, 24). Extracellular domains of FGFRs consist of three immunoglobulin-like loops (loop I, II, and III). Alternative mRNA splicing of loop III of FGFR1 to FGFR3 leads to distinct functional variants (IIIb and IIIc) that have different ligand-binding specificities and affinities. FGFR4 does not have alternative splicing but is most similar to an IIIc-like domain (1, 30, 31). Differential expression of IIIb and IIIc variants is very important for determining FGF signaling specificity. For example, the expression of FGFR2 isoforms of IIIb and IIIc is restricted to the cells of epithelial and mesenchymal lineage, respectively. In addition, exon switching from FGFR2IIIb to FGFR2IIIc was observed in progressive prostate cancer (32). FGF8 preferentially activates FGFR2IIIc and FGFR3IIIc splice forms and FGFR4 (17, 33), although there are differences between the activation potential of various FGF8 isoforms. FGF8b also activates FGFR1IIIc but only at a very high concentration (17). The receptors are activated through dimerization and phosphorylation by the intracellular tyrosine kinase domains (34). This process activates the Ras signal transduction pathway via FGFR substrate 2 (FRS2), the key components of which are the mitogen-activated protein kinases (MAPK) extracellular signal-regulated kinase (ERK) 1 ($p44^{MAPK}$) and ERK2 ($p42^{MAPK}$; for reviews, see refs. 35, 36).

We had already established a neutralizing monoclonal anti-FGF8b antibody, KM1334, by immunizing FGF8b-derived peptide. KM1334 was shown to inhibit androgen- and FGF8b-dependent growth of SC-3 cells *in vitro* (24). Furthermore, high frequency of FGF8 expression in clinical prostate cancers and breast diseases was immunohistochemically shown by KM1334 (24, 26), which is consistent with the results of immunohistochemistry and *in situ* hybridization reported by other groups (25, 27).

To investigate the potential of KM1334 as therapeutic agent for the treatment of cancers that are dependent on FGF8b signaling for growth and survival, we further evaluated its binding specificity, blocking activity, and *in vivo* antitumor activity. We show that KM1334 possesses high specificity and potent blocking activity *in vitro*. In addition, we show that this antibody exhibit strong antitumor activity *in vivo* mice model and its activity is mediated by both antiproliferative and proapoptotic activities.

Materials and Methods

Antibodies. A murine mAb against FGF8b, KM1334, was established as described previously (24). Briefly, the keyhole limpet hemocyanin–conjugated FGF8b peptide (FGF8b-1) from amino acid residues 23 to 46 of human and mouse FGF8b was used as an immunogen. A murine mAb, KM511, raised against a mutant of granulocyte colony-stimulating factor was described previously (37) and used as a negative control.

Anti-phosphospecific ERK1/2 rabbit polyclonal antibody and anti-phosphorylated FRS2α rabbit polyclonal antibody were obtained from Cell Signaling Technology (Beverly, MA). Anti-ERK2 mAb (clone 1B3B9) and anti-FRS2 rabbit polyclonal antibody (H-91) was purchased from Upstate Biotechnology (Lake Placid, NY) and Santa Cruz Biotechnology (Santa Cruz, CA), respectively. Anti-β-actin mouse mAb (ab8226) was from Abcam (Cambridge, United Kingdom).

Cells and animals. The SC-3 cell line used in the present study was derived from an androgen-responsive mouse mammary SC115 tumor (38). Adult male BALB/c *nu/nu* mice were purchased from Nippon Clea Co. (Tokyo, Japan).

Synthesis of fibroblast growth factor 8 fragment. Peptides with amino acid residues from 23 to 35 of human FGF8a (FGF8a-1), from 23 to 46 of human FGF8b (FGF8b-1), from 23 to 64 of human FGF8e (FGF8e-1), and from 23 to 75 of human FGF8f (FGF8f-1) were synthesized by an automated peptide synthesizer. For inhibition ELISA, FGF8b fragment (FGF8b-1) with additional cysteine residue in COOH terminus was synthesized and conjugated to bovine serum albumin (BSA).

Cross-reactivity of KM1334 to human fibroblast growth factor 8 variants (inhibition ELISA). The FGF8b-1 peptide conjugated to BSA was plated onto 96-well plate at a concentration of 1.0 μg/mL per 50 μL of each well. After overnight plating at 4°C, the plate was washed with PBS and blocked with 1% BSA in PBS. Then, the synthetic peptides, FGF8a-1, FGF8b-1, FGF8e-1, FGF8f-1, and a control peptide with a irrespective sequence (CGAGPKRRALAAPAAEEKEEA), were serially diluted and added into each well with KM1334 (final concentration, 0.08 μg/mL). After 2 hours of incubation at room temperature, the plate was interacted with horseradish peroxidase–labeled anti-mouse immunoglobulins (DAKO Corp., Carpinteria, CA) and 2,2′-azino-bis(3-ethylbenz-thiazoline-6-sulfonic acid substances, WAKO, Osaka, Japan). The absorbance at 415 nm was measured using an E-max microplate reader (Molecular Devices Corp., Sunnyvale, CA).

Cross-reactivity of KM1334 to human fibroblast growth factor 17b and fibroblast growth factor 18 (binding ELISA). Recombinant human FGF17b (R&D Systems, Inc., Minneapolis, MN), human FGF18 (R&D Systems), mouse FGF8b (R&D Systems), and human FGF2 (PeproTech, London, United Kingdom) were plated onto 96-well plate at serial concentrations from 0.1 ng/mL to 10 μg/mL per 50 μL of each well. After overnight plating at 4°C, the plate was serially washed and blocked with 1% BSA, and KM1334 was added into each well at a concentration of 1 μg/mL per 50 μL of each well. After washing, the bound antibody was detected as described previously.

Binding activity of fibroblast growth factor receptor-Fc fusion proteins to fibroblast growth factor 8b (binding ELISA). FGFRs fused with human IgG1 Fc domain (FGFR-Fc fusion proteins; human FGFR1IIIc-Fc, human FGFR2IIIc-Fc, murine FGFR3IIIc-Fc, and human FGFR4-Fc) were

purchased from R&D Systems. Production of a negative control, human interleukin (IL)-5 receptor (IL-5R)-Fc fusion protein, will be described elsewhere.[4] FGF8b was coated onto 96-well plate at a concentration of 5 μg/mL. After washing, the wells were incubated with serial concentrations of the FGFR-Fc and IL-5R-Fc fusion proteins. Bound FGFR-Fc fusion proteins on FGF8b were detected with anti-human IgG labeled with horseradish peroxidase (American Qualex, San Clemente, CA) diluted 1:12,500 as a secondary antibody. Inhibition of the FGF8b binding to FGFR-Fc fusion proteins by KM1334 was evaluated in this system. Serially diluted KM1334 or KM511 were added with each FGFR-Fc solution (10 μg/mL FGFR2IIIc-Fc, 2 μg/mL FGFR3IIIc-Fc, and 1 μg/mL FGFR4-Fc) to the FGF8b-coated plate. After washing, the secondary antibody bound to human Fc was detected as described previously.

Western blot. SC-3 cells were plated into 10 cm dishes at 2×10^6 cells per dish in a serum-supplemented medium; 2S(−) [Ham's F-12:DMEM (1:1, v/v) containing 2% dextran-coated, charcoal-treated fetal bovine serum] and allowed to adhere. After 8 hours of incubation at 37°C, the medium was exchanged with a serum-free medium; B0.1 [Ham's F-12:DMEM (1:1, v/v) containing 2% BSA] and incubated for 16 hours. Then, the medium was changed to an experimental medium composed of B0.1 and incubated for 15 minutes. After wash with PBS, cells were lysed in 500 μL lysis buffer [50 mmol/L HEPES-NaOH (pH 7.4), 250 mmol/L NaCl, 1 mmol/L EDTA, 1% NP40, 1 mmol/L DTT, 1 mmol/L phenylmethylsulfonyl fluoride, 5 μg/mL leupeptin, 2 mmol/L Na_3VO_4, 1 mmol/L NaF, 10 mmol/L β-glycerophosphate; ref. 39]. Cell lysates were clarified by centrifugation and total cell lysate (20 μg) from each sample was used for SDS-PAGE. After SDS-PAGE, the protein were transferred to polyvinylidene difluoride membranes and immunoblotted with appropriate secondary antibodies conjugated with horseradish peroxidase and developed using the enhanced chemiluminescence detection system according to the instructions of the manufacturer (Amersham Pharmacia Biotech, Piscataway, NJ).

Immunocytochemistry for SC-3 cells. SC-3 cells were inoculated into eight-well chamber slides (Nalge Nunc International, Rochester, NY) at 1×10^4 cells per well suspended in 200 μL 2S(−) medium and allowed to adhere. After 16 hours of incubation at 37°C, the medium was changed to an experimental medium composed of B0.1 and incubated for 24 hours. After wash with PBS, the chambers were removed and the slides were air-dried for 24 hours. Then, the cells were fixed in a 1:1 mixture of acetone/methanol for 10 minutes at room temperature. The slides were immunocytochemically stained for incorporated 5-bromo-2′-deoxyuridine (BrdUrd; Sigma Chemical Co., St. Louis, MO) labeling and terminal deoxynucleotidyl transferase–mediated nick end labeling (TUNEL) method (40). For BrdUrd labeling, BrdUrd was added to the medium at 100 μmol/L concentration for 1 hour before PBS wash. Then, the slides were treated with 3% H_2O_2 and 2 N HCl. BrdUrd incorporated into SC-3 cells was detected with a mouse anti-BrdUrd antibody (DAKO A/S, Glostrup, Denmark), EnVision, and 3,3′-diaminobenzidine (Merck, Darmstadt, Germany). Mayer's hematoxylin (Muto Pure Chemicals Ltd., Tokyo, Japan) was used for counterstaining. Positive cells and total cells in the three independent areas of 370 × 500 μm were counted. TUNEL method was done using the ApopTag Apoptosis *In situ* Detection Kit (Intergen, Purchase, NY) according to the manufacturer's instruction. Briefly, the slides were treated with 3% H_2O_2 and the nick ends of DNA were labeled with digoxigenin by terminal deoxynucleotidyl transferase enzyme. Apoptotic cells were detected with an anti-digoxigenin peroxidase conjugate using 3,3′-diaminobenzidine (WAKO) as a substrate. Mayer's hematoxylin was used for counterstaining. Positive cells and total cells in the three independent areas of 370 × 500 μm were counted. Statistical significances in the ratio of BrdUrd- or TUNEL-positive cells between the KM1334 group and the KM511 group were determined by two-tailed unpaired *t* test.

Evaluation of antitumor activity. All of the *in vivo* experiments were done in conformity with institutional guidelines in compliance with national laws and policies. SC-3 cells were harvested, washed with PBS, and inoculated s.c. in the dorsal side of male athymic nude mice by 1×10^6 cells per head suspended with 100 μL PBS. Tumors were allowed to reach ~300 mm^3 in size, and the mice were randomized into groups of five animals each. Mice were treated with KM1334 (50, 100, 200, and 400 μg in 200 μL PBS/mouse/shot) or PBS (200 μL/mouse/shot) by i.p. injection twice weekly. Treatment of animals was continued for the duration of the study (total of nine shots). Tumors were measured twice weekly with calipers, and tumor volumes were calculated by the following formula according to the methods of the National Cancer Institute (ref. 41; length and width of the tumors measured in mm): Tumor volume (mm^3) = (Length × $Width^2$) / 2.

Statistical significances in tumor size between the KM1334 group and the vehicle control (PBS) group were determined by two-tailed unpaired *t* test.

Immunohistochemistry for tumor sections. SC-3 cells were inoculated into athymic male nude mice according to the method written above. When SC-3 tumors reached 120 to 600 mm^3 in size, the mice were randomized into seven groups of three animals each. KM1334 and KM511 were given into three groups each by 400 μg in 200 μL PBS/mouse/shot. Tumors were collected at timings as follows: before antibody injection and at 7, 24, and 72 hours after antibody injection. Tumor volume was also measured immediately before each collection of tumors. One hour before tumor collection, BrdUrd dissolved in saline (20 mg/mL) was given i.v. into the mice by 100 mg/kg. The collected tumors were cut into two aliquots and were fixed in 10% neutral buffered formalin, embedded in paraffin, and sectioned at 3 μm. After deparaffinization and rehydration, sections were immunohistochemically stained for incorporated BrdUrd labeling and TUNEL method as described in immunocytochemistry of SC-3 cells (40). For BrdUrd labeling, sections were treated with 0.05% Pronase after neutralization with sodium borate. For TUNEL staining, sections were treated with proteinase K (Life Technologies, Rockville, MD) before digoxigenin labeling with terminal deoxynucleotidyl transferase enzyme. Positive cells in the area of 320 × 420 μm were counted. Statistical significances in BrdUrd- or TUNEL-positive cells between the KM1334 group and the KM511 group were determined by two-tailed unpaired *t* test.

Results

Binding specificity of an anti–fibroblast growth factor 8b monoclonal antibody, KM1334. To evaluate the therapeutic potential of an anti-FGF8b mAb KM1334, we first analyzed its specificity. We generated four synthetic peptides derived from human FGF8 variants (a, b, e, and f) and examined their inhibitory effect on the binding of KM1334 to its epitope-containing conjugate (FGF8b-1-BSA conjugate) in ELISA. Figure 1A and B show the structure of human FGF8 protein isoforms and the amino acid sequences of the synthetic peptides. Among the peptides examined, FGF8b-1 and FGF8f-1 significantly inhibited the binding of KM1334 to its antigen, indicating that KM1334 recognizes both FGF8b and FGF8f isoforms (Fig. 1C). On the other hand, FGF8a-1 and FGF8e-1 did not inhibit the binding. The lack of binding of KM1334 to FGF8a-1 is consistent with previously reported results (24). We next examined the cross-reactivity of KM1334 to FGF17b and FGF18, which are the closest members of FGF8 in FGF family, and their sequences corresponding to FGF8b-1 have significant homology with FGF8b (Fig. 2A). KM1334 showed strong binding to FGF8b; however, KM1334 did not bind to FGF17b,

[4] M. Koike et al. Anti-human IL-5Rα neutralizing monoclonal antibodies, manuscript in preparation.

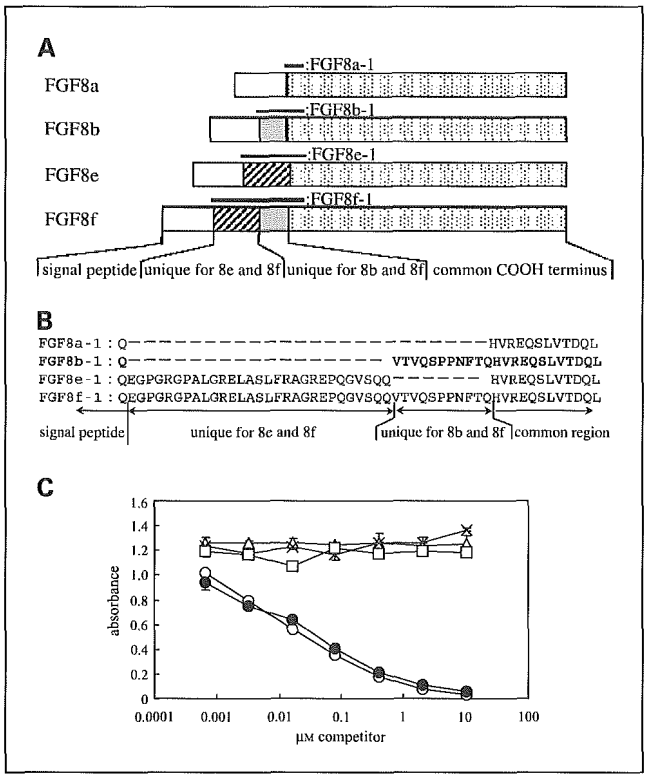

Fig. 1. Specificity of KM1334 to FGF8 variants. *A*, human premature FGF8a, FGF8b, FGF8e, and FGF8f protein isoforms, depicted NH_2 terminus (*left*) to COOH terminus (*right*). Solid bars above each columns, region used for synthetic peptides (*right*). *B*, alignment of amino acid sequences belonging to human FGF8 isoforms. FGF8a-1, FGF8b-1, FGF8e-1, and FGF8f-1 correspond to partial sequences of FGF8a, FGF8b, FGF8e, and FGF8f, respectively. KM1334 was raised against FGF8b-1 (*bold*) that includes unique sequence for FGF8b and FGF8f (VTVQSPPNFTQ). All four synthetic peptides were designed to contain the shared sequence (HVREQSLVTDQL) of all FGF8 isoforms. FGF8b-1 and FGF8f-1 contained unique sequence for FGF8b and FGF8f. FGF8e-1 and FGF8f-1 contained unique sequence for FGF8e and FGF8f. Gaps were introduced to facilitate understanding of the identity among each sequence. *C*, inhibition ELISA to analyze binding specificity of FGF8 variants: FGF8b-1 (○; positive control), FGF8f-1 (●), FGF8a-1 (△), FGF8e-1 (×), and peptide for negative control (□). Points, mean for $A_{415\text{-}490}$; bars, SD.

FGF18, and FGF2 (Fig. 2B). These results show that KM1334 possesses the high specificity to FGF8b.

Neutralizing activity of KM1334. Since Tanaka et al. reported that KM1334 inhibited SC-3 growth *in vitro* (24), direct evidence of blocking activity of KM1334 has not been shown yet. We first examined the binding of FGF8b to FGFR-Fc fusion proteins (FGFR1IIIc-Fc, FGFR2IIIc-Fc, FGFR3IIIc-Fc, and FGFR4-Fc) in ELISA. Among FGFR-Fc fusion proteins tested, FGFR2IIIc-Fc, FGFR3IIIc-Fc, and FGFR4-Fc showed significant binding activity to FGF8b; however, FGFR1IIIc-Fc showed little binding to FGF8b (Fig. 3A). The order of affinity was as follows: FGFR4-Fc ≧ FGFR3IIIc-Fc > FGFR2IIIc-Fc. The apparent affinities of FGFR4-Fc and FGFR3IIIc-Fc with FGF8b were 32.2- and 11.3-fold higher than that of FGFR2IIIc-Fc, respectively. Then, the ability of KM1334 to block the FGF8b binding to FGFR-Fc fusion proteins was assessed in this ELISA. KM1334 blocked the binding of FGF8b to all the FGFR-Fc fusion proteins examined: FGFR2IIIc-Fc (IC_{50}, 0.31 μg/mL; Fig. 3B), FGFR3IIIc-Fc (IC_{50}, 0.86 μg/mL; Fig. 3C), and FGFR4-Fc (IC_{50}, 0.95 μg/mL; Fig. 3D). Control antibody KM511 did not show any blocking activity.

To identify FGF8b-stimulated signal transduction pathway in SC-3 cells, phosphorylation of FRS2α and MAPK (ERK1/2) was examined in Western analysis. Phosphospecific antibodies against FRS2α and ERK1/2 gave stronger signal to FGF8b-stimulated cells than nonstimulated control cells. The expression level of ERK2 was almost the same in all samples (Fig. 4A). On the other hand, FRS2 expression seemed to be up-regulated slightly in the FGF8-stimulated cells. KM1334 inhibited FGF8b-induced phosphorylation of both FRS2α and ERK1/2 in a dose-dependent manner (Fig. 4A).

Furthermore, immunocytochemical analysis revealed that FGF8b promotes uptake of BrdUrd and rescues apoptosis in SC-3 cells, which show that FGF8b is critical for the growth and survival of SC-3 cells. KM1334 also inhibited those effects in a dose-dependent manner (Fig. 4B and C), which was in agreement with a previous report demonstrating that KM1334 inhibited FGF8b- and androgen-dependent growth of SC-3 cells (24). These results indicate that KM1334 possesses the potent *in vitro* neutralizing activity.

In vivo *effect of KM1334 on SC-3 tumors in mice.* We next examined the potential of antitumor activity of KM1334 on the growth of SC-3 tumor implanted on nude mice. SC-3 cells were injected into male nude mice s.c. and allowed to grow to ~300 mm^3 in size. Antibody treatment of 50, 100, 200, and 400 μg/injection was started 10 days after tumor inoculation and the tumor sizes were monitored until day 38. As shown in Fig. 5, treatment with KM1334 resulted in dose-dependent suppression of SC-3 tumor growth. On day 38, at the end of the experiment, the treated versus control values (i.e., relative volume of treated tumors divided by the relative volume of control tumors × 100) of 50, 100, 200, and 400 μg treated groups were 60%, 53%, 19%, and 4.3%, respectively. Rapid regression of SC-3 tumors were observed in the maximum dose group of KM1334 (400 μg/injection).

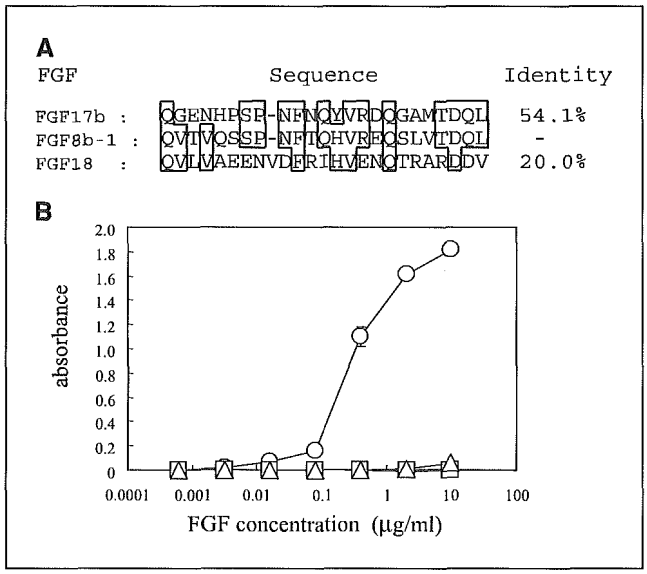

Fig. 2. Specificity of KM1334 to other members of FGF family with high homology to FGF8. *A*, alignment of amino acid sequences of FGF17b and FGF18 with FGF8b. Gaps were introduced to optimize the homology. Boxed area, shared residues in more than two FGFs. *B*, binding ELISA to detect cross-reactivity of KM1334 to other FGFs. A ELISA plate was coated for FGFs [i.e., FGF8b (○), basic-FGF (◆; negative control), FGF17b (△), and FGF18 (□)] at various concentrations and KM1334 was reacted to them at 1.0 μg/mL. Points, mean for $A_{415\text{-}490}$; bars, SD.